Ore Geology Reviews 106 (2019) 387–402

Contents lists available at ScienceDirect

Ore Geology Reviews

journal homepage: www.elsevier.com/locate/oregeorev

The geology and mineralization of the Long Chieng Track (LCT) subvolcanic Au-Ag-Cu-Pb-Zn deposit, Lao PDR

Peter Leaman[a,*], Takayuki Manaka[b,1], Kristalyn Jarical[c], Michael Villar[d], Jose B. Libao[d]

[a] PanAust, Level 1, 15 James Street, Fortitude Valley, Brisbane, Queensland 4006, Australia
[b] CODES Centre of Ore Deposit and Earth Sciences, University of Tasmania, Hobart, Tasmania 7001, Australia
[c] PanAust Services (Myanmar), Sakura Tower, 339 Bogyoke Aung San Road, Yangon, Myanmar
[d] Phu Bia Mining, 7th Floor, Capital Tower, 23 Singha Road, Saysetha District, Vientiane, Lao Democratic People's Republic

A B S T R A C T

The Long Chieng Track deposit contains a mineral resource of 32 Mt @ 0.77 g/t Au + 4.9 g/t Ag + 0.12% Cu. It is described here as a subvolcanic polymetallic Au-Ag-Cu-Pb-Zn deposit occurring within a folded and faulted Permian age volcanosedimentary formation in the Truong Son Fold Belt of north-central Laos. The geological sequence is interpreted to have formed in a subduction related arc environment. Mineralization is associated with dacitic porphyritic dykes and small stocks which were intruded into a sequence of volcaniclastics, carbonaceous sediments, sedimentary breccias, and limestones. Age dating by U-Pb geochronology of the dacitic porphyry unit yielded an intrusion age of 279 ± 4 Ma. Whole rock chemical analysis demonstrates that the rock suites are classified as I-type calc-alkaline series with elevated levels of alkali elements.

Mineralization at LCT occurs predominantly as stockwork veins which are spatially associated with the dacitic intrusions. The veins may be classified into main four types including undifferentiated (VNN), base metals (BMV), massive pyrite (MPY) and buck (BUK) veins. All vein types are mineralized except the BUK veins. Cross-cutting and overprinting relationships indicate that the VNN and BMV veins were formed earlier than the MPY veins. The dominant sets include steep NNE dipping (66°/010°) and steep NNW dipping (70°/340°) veins, and shallow to moderate SSE dipping veins (21°/172°). The majority of high gold grades are hosted within the VNN veins which predominantly dip to the SSE. In contrast, lead and zinc are dominant in the BMV veins, while the highest copper grades are mainly hosted in steep NNE and NNW dipping MPY veins. Ore minerals include pyrite, galena, sphalerite, chalcopyrite, electrum and native gold with minor arsenopyrite and molybdenite. Gold occurs either as electrum or native gold grains or as inclusions in pyrite.

Five distinct alteration phases are recognized: (1) quartz-adularia-sulfide; (2) sericite-quartz-pyrite-carbonate ± chlorite (3) Fe carbonate; (4) epidote-carbonate-chlorite; (5) kaolin-halloysite ± alunite. Phases 1 to 4 are generally progressively zoned from the deposit centre to the periphery. Phase 5 is associated with late steam-heated hot spring alteration and weathering and oxidation.

The field geology relationships suggests that the depth of formation can be estimated to be approximately 1–3 km below the paleo-surface.

The style of mineralization and geological relationships of the LCT deposit are similar to those described in other deposits formed in the transitional zone between the porphyry and epithermal environments. Therefore, we consider that sub volcanic style is the most appropriate environment to characterize the LCT deposit.

1. Introduction

The Long Chieng Track (LCT) deposit is located at 18°55′45″ N and 102°52′5″ E in the Xaisomboun Province of northern Lao PDR (Laos) some 210 km by road north of the capital city of Vientiane, approximately 7 km northeast of the Phu Kham mine and 25 km west of Xaisomboun Township.

Laos has a tropical monsoon climate with a rainy season from May to November and a dry season from December to April. Annual rainfall averages 200 mm in the area and maximum and minimum daytime temperatures range between 31 and 18 °C. The LCT deposit lies at an elevation of 850 m asl within generally rugged terrain. Vegetation consists of primary subtropical forest which has extensively been replaced by secondary bamboo growth as a result of slash and burn agriculture.

The LCT deposit lies within the Mineral Exploration and Production Agreement (MEPA) concession which was granted to Phu Bia Mining Ltd. (PBML) in July 1994. PBML is a joint venture company 90% owned by PanAust and 10% by the Government of Laos. The concession currently covers an area of 2637 km^2. Active mining operations were developed by PBML in 2005 at Phu Kham initially with a heap leach Au operation with production of Cu-Au concentrate commencing in 2008, and Au-Ag ore from the Ban Houayxai operation in 2012. Exploration continued at LCT with the objective of defining a deposit which could be developed either as a standalone operation or as a satellite deposit for Phu Kham or Ban Houayxai. These efforts resulted in the definition

* Corresponding author at: PanAust, Level 1, 15 James Street, Fortitude Valley, Brisbane, Queensland 4006, Australia.
E-mail address: peter.leaman@peterleamandiscovery.com.au (P. Leaman).
[1] Geological Survey of Japan, AIST, Central 7, 1-1-1 Higashi, Tsukuba, Ibaraki 305-8567, Japan.

https://doi.org/10.1016/j.oregeorev.2019.02.010
Received 23 October 2018; Received in revised form 22 January 2019; Accepted 12 February 2019
Available online 13 February 2019
0169-1368/

of a resource of 32 Mt @ 0.77 g/t Au + 4.9 g/t Ag + 0.12% Cu at a cut-off grade of 0.3 g/t Au (PanAust, 2014).

A comprehensive geological description of the LCT deposit occurring in a poorly known geologic terrain has to date not been published. This paper seeks to combine and review exploration data collected and developed over many years by PBML geologists, including research information completed at the University of Tasmania (Manaka, 2008).

2. Study methods

2.1. Whole rock geochemistry analytical method

A total of 14 samples from the LCT deposit were analyzed for the major (Si, Ti, Al, Fe, Mn, Mg, Ca, Na, K and P) and trace (Rb, Sr, Ba, Sc, V, Cr, Ni, Zn, Y, Zr, Nb and Pb) elements using X-ray Fluorescence (XRF) at CODES, the University of Tasmania. The detailed analytical technique is outlined by Norrish and Chappell (1977) and Norman et al. (2003). Rare earth elements (REE: La, Ce, Pr, Nd, Sm, Eu, Gd, Tb, Dy, Ho, Er, Tm, Yb and Lu) for six of these samples were also analyzed using the solution ICP-MS technique at the University of Tasmania. The detailed analytical method for the solution ICP-MS technique is described by Yu et al. (2000). To obtain reliable results, samples for the analyses were carefully selected from the least altered hand specimen samples. They were initially crushed using a jaw crusher to make rock fragments several centimeters in size and were subsequently ground using a tungsten carbide rig mill to produce rock powder.

2.2. Zircon U-Pb dating analytical method

A U-Pb zircon geochronological study was conducted on the major igneous units of the LCT deposit, using Laser Ablation Inductively Coupled Plasma Mass Spectrometry (LA-ICPMS) at CODES laboratory, University of Tasmania. The study aimed to constrain the age of igneous activity at LCT, in particular for the intrusions linked to the mineralizing event.

For this study, zircon crystals were separated from the feldspar-phyric dacitic porphyry, quartz monzonite and quartz monzodiorite. Zircon crystals were physically separated by crushing, milling and panning followed by microscopic selection of individual crystals. The separated zircon crystals were mounted in epoxy-resin disks and were polished. A number of zircon crystals (> 15 zircons) from the feldspar-phyric dacitic porphyry and quartz monzonite units were also identified and separated.

Prior to LA-ICPMS analysis the zircon crystals were examined with a microscope and cathodoluminescence (CL) images were acquired on some samples to characterize the zircon crystals. The shape of zircon crystals offers important clues as to the origin of the crystals (Corfu et al., 2003). Most of the zircon crystals separated for this study are of igneous origin as shown by well-developed internal crystal-growth zoning in the crystals.

LA-ICPMS U-Pb zircon analysis (Kosler and Sylvester, 2003) was conducted using U and Pb isotopic composition for each of the separated zircon crystals. They were ablated in a He atmosphere in a custom-made chamber at 5 Hz and 30 μm. The primary standard, the Temora standard zircons (Black et al., 2003) were analyzed four times each hour, and additional secondary standard zircons ranging from 2.6 to 1063 Ma in age were analyzed to check the precision and accuracy of the results. For a more detailed description of the analytical method, see Meffre et al. (2007).

3. Geologic and tectonic setting

3.1. Regional geology and Cu-Au deposits

The MEPA concession lies at the intersection of the Truong Son and Loei-Petchabun volcano-plutonic Fold Belts which developed during the Paleozoic and Mesozoic eras (Fig. 1). Nearly all the significant Cu-Au mineral deposits of mainland Indochina occur within these belts (Goldfarb et al., 2014; Zaw et al., 2014). These include the Chatree Au-Ag low sulfidation epithermal (Salam, 2013) and Puthep Cu-Au porphyry/skarn (Puthep Company limited, 2009) deposits in Thailand, and the Sepon Cu-Au mineral field (Cromie, 2010; Cromie et al., 2018) and Phu Kham Cu-Au porphyry/skarn (Tate, 2005; Kamvong, 2013), Ban Houayxai Au-Ag epithermal (Manaka, 2008; Manaka et al., 2014), LCT Au-Ag-Cu-Pb-Zn (in this paper) and the Kham Thong Lai (KTL) Cu-Au skarn related (Merriner, 2013) deposits in Laos.

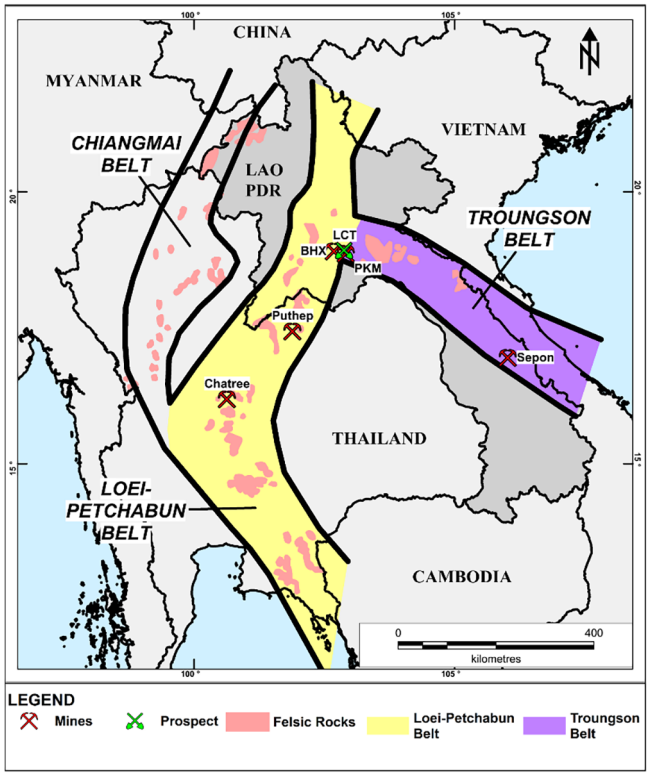

Fig. 1. The relationship of the Truong Son and Loei-Petchabun Fold Belts and the location of active Cu-Au and Au-Ag mining operations and significant mineral deposits. Adapted from Tate (2005). Abbreviations; PKM = Phu Kham, BHX = Ban Houayxai.

The Truong Son Fold Belt (TSFB) trends northwest from central Vietnam to northern Laos and forms the northern part of the Indochina terrane of mainland Southeast Asia (Zaw et al., 2014). It is a structurally complex Paleozoic fold belt consisting of Ordovician and Silurian age igneous, metamorphic and sedimentary rocks occurring in various geologic sub-domains with later successor basins ranging in age from Silurian to Permian (Lepvrier et al., 2004). The sub-domains have been displaced by dextral transpressional northwest-southeast trending faults formed during the Indosinian thermotectonic event between 250 and 240 Ma (Lepvrier et al., 2004). Late Triassic northeast-southwest extension produced northwest-trending half-grabens of regional extent.

Evidence of early Permian arc mafic-felsic magmatism extends from central Yunnan in southwest China at least to the Phonsavan District in Xieng Khouang Province in northern Laos, although the location of the related subduction zone is unknown. In Laos this belt consists predominantly of plagioclase phyric andesitic volcanics overlying carboniferous limestone and siliciclastic sedimentary rocks (Hotson, 2009; Fig. 2). Calc-alkaline granitoids are distributed throughout the TSFB but are more abundant in the northwestern region (Hoa et al., 2008) and are regionally associated with mineralization. The Loei-Petchabun Fold Belt (LPFB) is structurally less complex with a distinct zoning of Devonian-Triassic volcanic rocks in the north part of the belt trending to

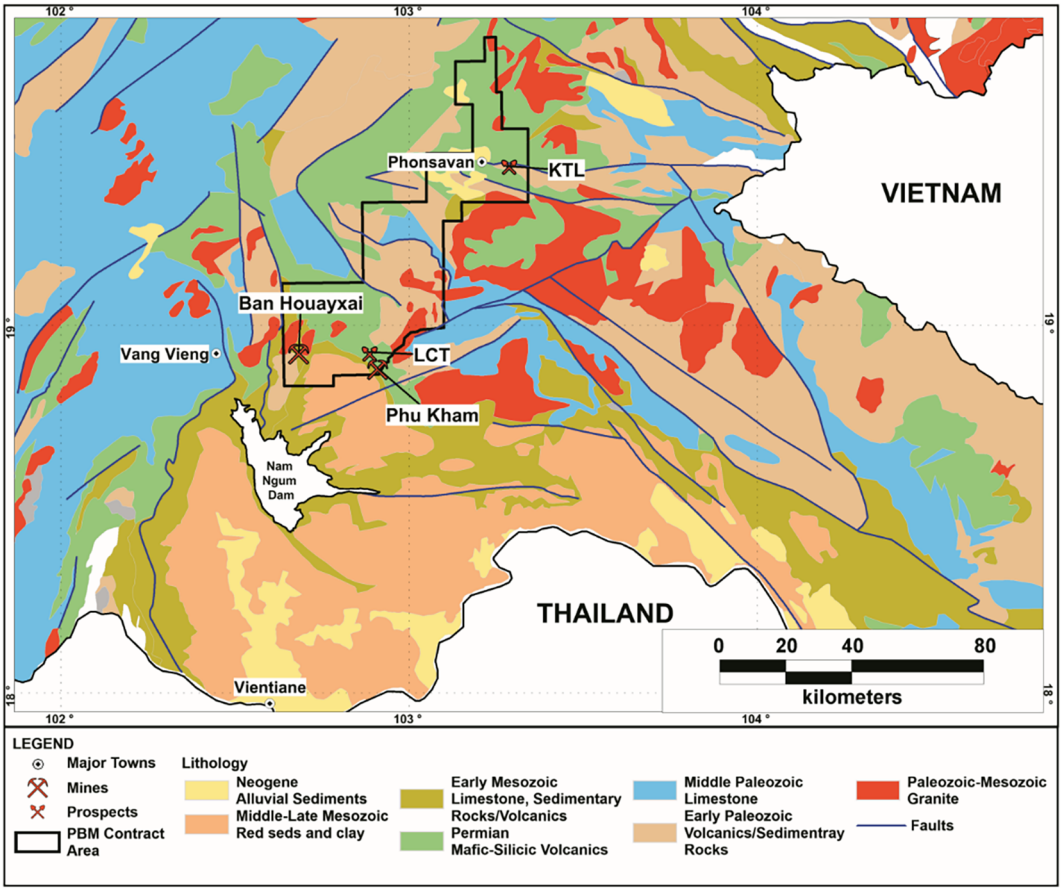

Fig. 2. The geology and major structures of the northwest Truong Son foldbelt and the location of the major deposits within the MEPA concession. Map adapted from British Geological Survey (1990) and GIS data from the CODES-Industry Project (2014).

younger Cainozoic volcanics in the central and southern zones (Intasopa et al., 1995). Former geochronological studies to confine timing of mineralization of the Phu Kham, Ban Houayxai and KTL deposits in the MEPA concession indicated that they are genetically linked to Late Carboniferous-Early Permian (310–260 Ma) magmatism of the TSFB, rather than that of the LPFB which is confined to the Late Permian-Jurassic period (e.g., Zaw et al, 2014). Mineralization at the LCT deposit is therefore considered by the authors to be part of the Late Carboniferous-Early Permian metallogenic event resulting from the subduction-collision event of the Indochina and South China Terranes during the Early Permian (Zaw et al., 2014; Shi et al., 2015).

3.2. Geology of the MEPA concession

The geology of the MEPA concession includes various sedimentary and igneous rock types (Fig. 2). The oldest rocks within the concession area are metasediments which tectonically underlie the Middle Silurian granite at Phu Kham and have only been intersected in drillholes. The metasediments have a maximum Neoproterozoic depositional age based on U-Pb dating of detrital zircons (youngest zircon ages of 597 ± 7 Ma; Gain and Gréau, 2013; Cairns, 2013). The oldest outcropping rock unit currently known within the concession is a large body of granite east of the Phu Kham deposit, reported by Backhouse (2004) as being Middle Silurian in age. This granite has been interpreted by Tate (2005) to be structurally juxtaposed against very thick and regionally extensive karstic limestone of which the timing of faulting and the age of the limestone remains unknown. The granite may potentially represent an exhumed core complex or more likely a batholith exposed by thrusting and erosion.

Late Silurian-Devonian age sandstones and siltstones with intermittent and calcareous units occupy the majority of the concession central area but are barren of mineralization. The oldest fossil to be recovered is *Icriodus symmetricus*, of Late Devonian (Frasnian) age from an area of limestone located north of LCT (Cairns, 2013).

Late Carboniferous-Early Permian volcaniclastics occur extensively throughout the southern and northern areas of the concession. These largely comprise volcaniclastic sediments and volcanic flows and breccias which are generally intermediate to felsic in composition with minor mafic flows. There is some evidence of several volcanic cycles, each accompanied or followed by an intrusive event usually consisting of diorites, tonalities, and monzonites with late stage feldspar porphyry dykes. Whole rock geochemistry completed to date suggests that the Early Permian igneous rocks are of calc-alkaline affinity emplaced in a continental-arc setting (Backhouse, 2004; Manaka, 2008; Hotson, 2009; Kamvong, 2013). All significant mineral occurrences are hosted within the volcaniclastics and appear to be associated with the Early Permian intrusive events. The thickness of the Early Permian volcaniclastic sequence is yet to be firmly established but is estimated to be between 1 and 3 km thick.

The volcaniclastics are overlain by a Permian Limestone unit and Undifferentiated Sediments that occupy the central zone of the concession. The latter consists predominantly of sandstones and minor siltstones and calcareous units. The limestones typically form a prominent karst topography.

The youngest consolidated rock unit identified to date is the Red Sediments which is located along the southern boundary of the tenement between the Phu Kham and the Ban Houayxai deposits. It has a maximum mid-Triassic depositional age of 246 ± 4 Ma based on detrital zircon age (Cairns, 2013). A thrusted unconformity separates the continental derived Red Sediments from the Early Permian

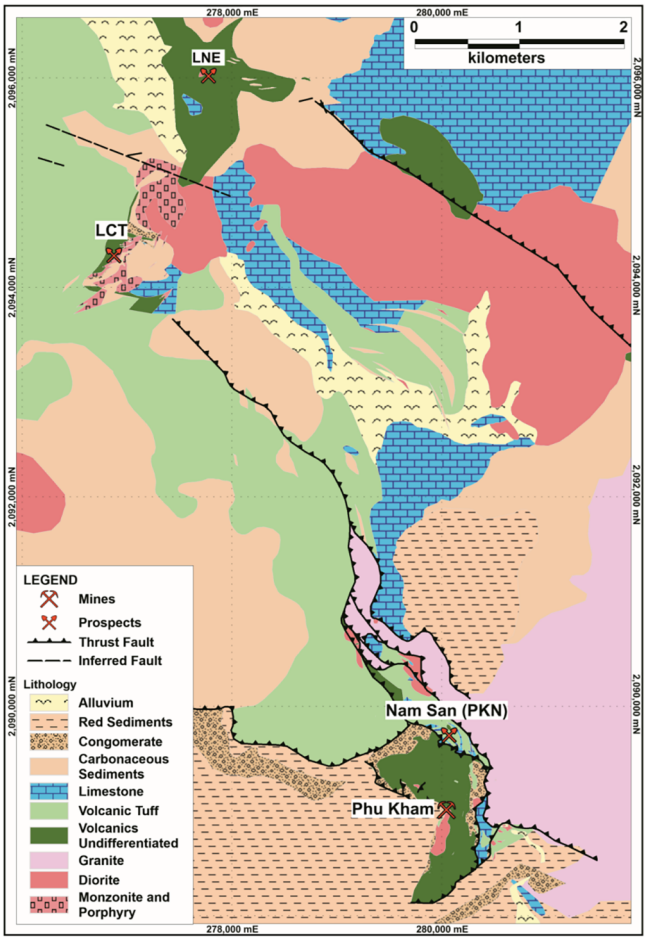

Fig. 3. Simplified geology map of the northern Phu Kham district based on field mapping and interpretation of regional helimagnetic survey data. Southwest verging thrusting results in stacking of older units upon younger units and duplex stacking within individual units. The relative positions of Phu Kham and LCT are shown. The Nam San (PKN) deposit is described in Leaman et al. (2015).

volcaniclastic sequence immediately to the north.

3.3. Structure

The TSFB was subjected to increasingly intense compression and crustal shortening during the Indosinian Orogeny which commenced during the Permian and culminated during the Triassic. The Indosinan Orogeny is currently poorly time constrained but considered to have occurred between 200 and 250 Ma (Lepvrier et al., 2004; Lin et al., 2007; Carter and Clift, 2008). This event resulted in several phases of thrusting and folding as evidenced by folded thrust surfaces in the southwest of the MEPA concession (Cairns, 2013; Fig. 3). The two most significant phases of thrusting are north and NE-directed and consist of a regional series of thrusts that within individual formations may result in duplex and imbricate thrust faulting (Cairns, 2013). The north directed thrust event is interpreted to have occurred in the syn-post Triassic given that Middle to Late Paleozoic rocks have been thrusted over the Late Triassic Red Sediments. The most continuous north directed thrust surface is that separating the mineralized Late Carboniferous-Early Permian volcaniclastics and the Triassic Red Sediments at the southern margin of the existing concession area. The northeast directed thrusts are evidenced by a dominant east-west striking moderate north dipping foliation that is interpreted to have formed in response to this phase of thrusting (Farmer et al., 2013), which suggests they are younger than the north directed set.

At least two phases of folding have been recognized within the Phu Kham deposit, which reflect regional folding events from Late Carboniferous to Late Cretaceous (Tate, 2005). The dominant fold event consists of open to tight east-west trending regional folds which must post date north directed thrusting with folding of those structures. A second north-south trending fold event is primarily evidenced in the Red Sediments but is less common in the older rocks (Cairns, 2013).

Three later faulting events are evidenced by northeast trending strike/oblique-slip predominantly sinistral brittle faults that offset the north directed thrusts and stratigraphy. They are delineated primarily by interpretation of regional airborne magnetics and can be traced for distances of up to 25 km. The youngest and third fault set is strike slip and trends west-northwest and crosscuts older structures.

3.4. Exploration history

The initial owners of PBML were the Government of Laos and Normandy Anglo Asian Pty Ltd. The latter consisted of a consortium of Anglo American Corporation, Normandy Poseidon Ltd and Poseidon Gold Ltd which managed the project between 1994 and 2002. The consortium was focused on the discovery of Au deposits, and other commodities were of secondary interest only. The original MEPA concession covered an area of 5000 km^2 and regional geochemical sampling surveys were completed in several phases. These programs included the collection of a bulk cyanide leach (BCL) and a conventional < 80 mesh sediment samples at each site. Access to some areas was initially restricted because of contemporary security issues, but an improving situation eventually allowed for the area to be sampled to an acceptable density by late 1996. The LCT geochemical anomaly was identified during this program, defined by regional Au and Ag stream sediment BCL anomalies and anomalous Ag and Pb in < 80 mesh samples. The MEPA boundaries were renegotiated at this stage and the concession subsequently reduced to an area of 2450 km^2.

Follow-up ridge and spur sampling of the B zone horizon of the residual soil profile outlined a significant geochemical Au anomaly. In 1996–97 a program of 25 shallow scout diamond drillholes (totaling 2715 m) was completed to test the oxide zone. The potential for the discovery of a large resource was considered to be low and no further exploration was completed (Wroe, 1997).

PanAust acquired a controlling interest in PBML in April 2002 and targeted the LCT oxide zone for material which could be used as ore for a heap leach operation. Between 2003 and 2006 a total of 124 reverse circulation and six diamond drillholes were subsequently completed. A small resource was defined but the material was considered unsuitable as heap leach feed. No further drilling was done until 2011 when six additional diamond drillholes were completed to target higher grade zones. Rising commodity prices resulted in a decision to drill out the primary mineralization on a nominal 50 m × 100 m spaced grid, and 99 diamond drillholes were completed for 35,479 m between 2011 and 2013. Soil sampling programs completed at the LCT Northeast prospect (LNE) identified geochemical anomalies which were tested with nine drillholes for 3117 m which identified a system considered to be a distal extension of the main LCT deposit (Fig. 4). Overall a total of 259 drillholes for a combined 48,814 m were completed by the end of 2013. The defined resource at LCT of 32 Mt @ 0.77 g/t Au and 4.9 g/t Ag is currently considered to be uneconomic and subsequent work has been limited to understanding the deposit geology.

4. Deposit geology

4.1. Stratigraphy and lithologic units

The geology of the LCT deposit area consists of a thick (> 500 m) sedimentary sequence which is characterized by abundant volcanic components in the upper part of the succession, and the sequence is intruded by few differentiated intrusive units (Fig. 5). The geology and

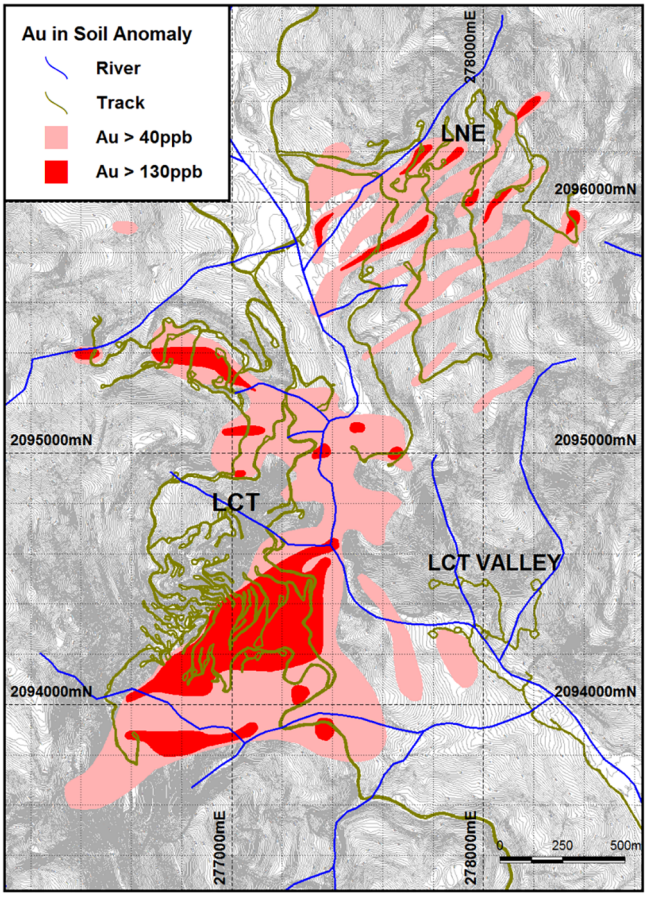

Fig. 4. Au-in-soil geochemical contours over the LCT and LNE prospects. At LNE the contours define the mineralized quartz veins are well defined at surface by the anomalous Au geochemistry.

stratigraphy are shown in Fig. 5A and B, and a cross-section is displayed in Fig. 5C.

The oldest unit in the succession is the Carboniferous Limestone consisting of bedded carbonaceous and calcareous limestone with minor shales/siltstones/sandstones. The limestone is dark grey and fine-grained in texture due to the presence of abundant carbonaceous material (Fig. 6A). Fossil fragments are common including Carboniferous age rugose corals (Cann, 1997) indicating a shallow depositional environment. The unit does not outcrop within the immediate LCT area but has been intersected in several diamond drillholes and the thickness is estimated as several tens of meters.

Carbonaceous Sediments consisting of alternating beds of sandstone and siltstone occur in the middle of the sedimentary sequence above the Carbonaceous Limestone unit. The lower part of the unit consists mainly of siltstone, whereas the upper part is sandstone dominated. These beds occur as layers from one to several tens of centimeters thick. In hand specimen the siltstone is dark and consists of carbonaceous materials whereas the sandstone displays discrete feldspar minerals (Fig. 6B).

The Sedimentary Breccia unit in the northern zone of the deposit is intercalated within the Carbonaceous Sediments unit. In hand specimen the breccias display a clast supported polymictic (carbonaceous, chloritic and siliceous fragments) texture with angular to sub-rounded clasts averaging 2–3 cm in size (Fig. 6C). The matrix is commonly cemented by fine-grained carbonate minerals (Mason, 1997).

The Volcanic Breccia and Undifferentiated Volcaniclastics units overlie the Carbonaceous Sediments unit, and are important hosts of mineralization. The Volcanic Breccia consists mainly of volcanolithic sandstone grading into a granulitic conglomerate. Clasts are predominantly andesitic and dacitic in composition with an abundance of fine-grained volcanic glass (Crawford, 2013). Most clasts are sub-angular and show little rounding (Fig. 6D) and are interpreted to have been derived from a proximal volcanic provenance.

The Undifferentiated Volcaniclastics unit is comprised of intermixed volcaniclastic siltstones and sandstones including lithic and crystal clasts and is widely distributed in the central part of the deposit. A crystal lithic tuff is the most common lithology and has a glassy, strongly plagioclase-phyric dacitic to andesitic lava composition and contains mainly lithic and sericitized plagioclase phenocryst clasts 1–4 mm across in a pale grey green matrix displaying a strong anastomosing foliation (Fig. 6E). Lithic carbonaceous fragments between 1 and 3 cm in size may be present and the matrix is very heterogeneous with common leucoxene granules suggesting that vitric ash might have been a significant matrix component (Crawford, 2013). The volcaniclastic sandstones in the unit are mainly sandstone to granulitic conglomerates with abundant lithic clasts of fine-grained mainly quenched and formerly glassy andesitic to felsic lavas. Most of these rocks are poorly sorted with a matrix rich in vitric ash that has devitrified and recrystallized to very fine-grained quartzo-felspathic intergrowths.

The Volcanic Tuff unit occurs dominantly in the central to western part of the deposit and unconformably overlies the Undifferentiated Volcaniclastics. The unit is interpreted to be the top of the succession at LCT, and consists of mixed tuffaceous sandstones and siltstones with variable amounts of crystal and lapilli clasts. This unit displays strong sericite-chlorite alteration with well-developed tectonic foliation (Fig. 6F).

Three intrusive units are identified at the LCT deposit, including quartz monzonite, quartz monzodiorite and feldspar-phyric dacitic porphyry. Characteristics of the units are described below and summarized in Table 1.

4.1.1. Quartz monzonite (P1a)

Quartz monzonite bodies represent the earliest intrusion phase and occur in the southern and northeastern zones of the deposit. They display a porphyritic texture consisting of sparsely distributed lath-shaped K-feldspar (20–30%) phenocrysts up to 5 mm in size with a pale greyish granular fine-grained groundmass (Fig. 7A). Minor mafic minerals are also present (10–15%) and are usually altered to chlorite. Fine-grained varieties range in mineralogical composition from quartz monzonite to monzonite, with the latter typically present as fine–grained micromonzonite dykes intruding coarser-grained quartz monzonites. In thin section sparsely distributed phenocrysts consisting of K-feldspar (50–60%), plagioclase (30–40%) and quartz (up to 10%) occur, usually as euhedral laths up to 5 mm (2–3 mm average) in size (Fig. 7B). Sericite alteration of the feldspars is patchy. Trace biotite (maximum 5%) is present and is usually replaced by chlorite and calcite. Groundmass alteration minerals include calcite, chlorite and clay minerals.

4.1.2. Quartz monzodiorite (P1b)

Quartz monzodiorite occurs in the northeastern zone but does not outcrop and is intersected only in drillholes. Hand specimens display a texture consisting of interlocking sub-millimeter sized grains of feldspar, biotite and euhedral pyrite (Fig. 7C). In thin section the phenocrysts are interlocked and consist of euhedral to tabular feldspars (60%), quartz (10%) and chlorite (20%). The feldspars are mainly plagioclase (80%) with minor K-feldspar (20%) (Fig. 7D). Chlorite commonly replaces biotite and pyrite and is evenly disseminated.

The contact relationships between this unit and quartz monzonite are complex, as the quartz monzodiorite appears to intrude the quartz monzonite but examples with opposite timing are also present. Thus, from these field relationships the quartz monzonite and quartz monzodiorite are considered to be broadly comagmatic.

4.1.3. Feldspar-phyric dacitic porphyry (P2)

These rocks typically occur as small stocks and dyke-like bodies

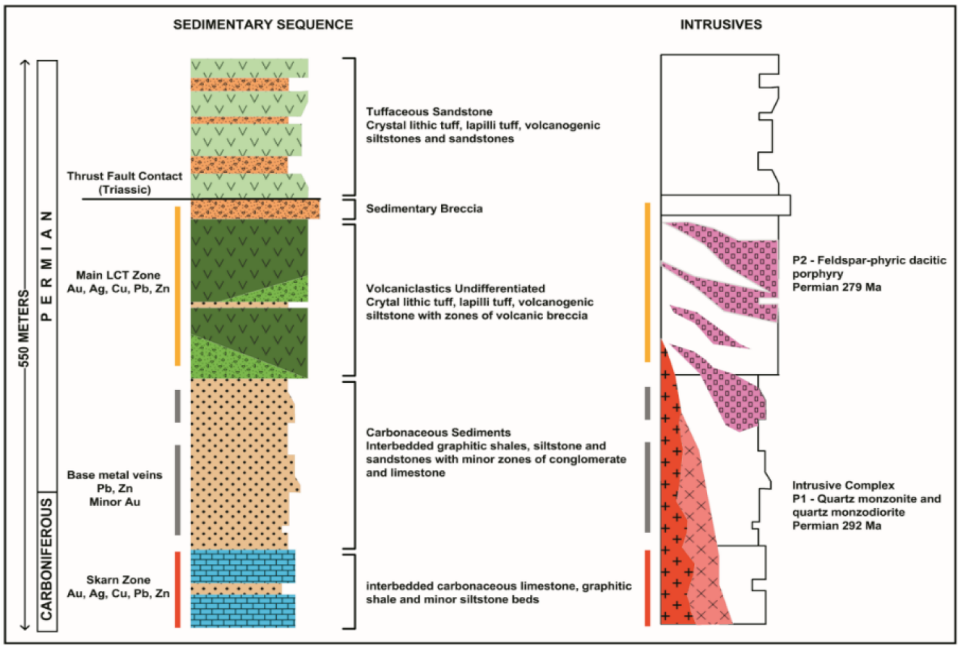

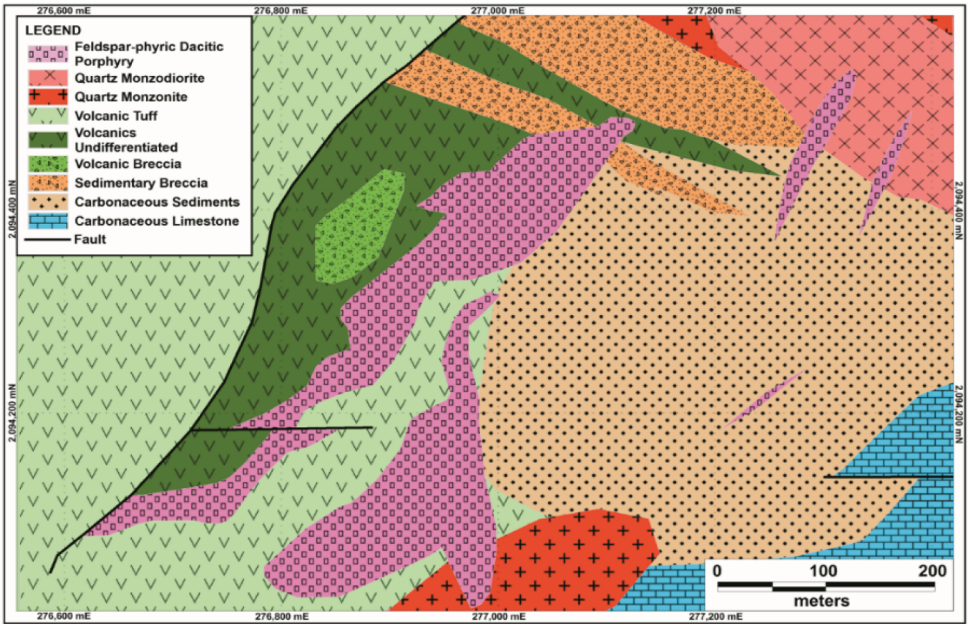

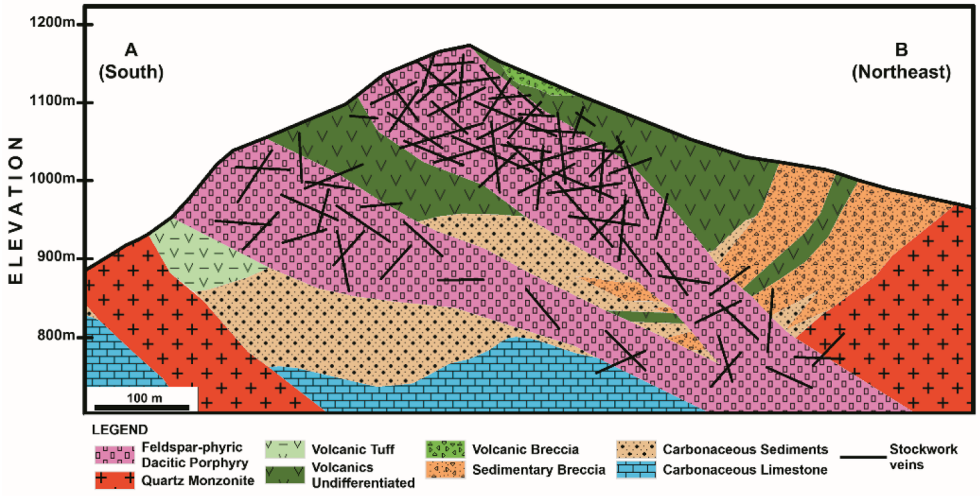

(caption on next page)

Fig. 5. Geology of the LCT deposit. A. Simplified interpreted stratigraphy (top). B. Surface geology (middle). C. Cross-section (bottom). Geological information is after Johnston (2002) and Tate (2003).

with an E-NE trend and steep northerly dips. They host the majority of mineralization. No clear field relationship with quartz monzonite and quartz monzodiorite has been observed, though geochronological data suggest this unit postdates the quartz monzonite. In hand specimen these intrusions have a porphyritic texture with milky colored uneven-sized phenocrysts (30–40%) in a greenish colored fine-grained matrix (Fig. 7E). Petrographic examination by Mason (1997) identified plagioclase (10–15%) and K-feldspar (40%) phenocrysts with primary quartz (10–20%) in the matrix, although most plagioclase has subsequently been altered to secondary adularia (Fig. 7F). Euhedral to subhedral K-feldspar phenocrysts commonly occur as single crystals, ranging from 0.5 to 2 mm in size. Hornblende (up to 10%) is the dominant mafic mineral and is largely replaced by chlorite. The groundmass is composed of fine-grained minerals including primary K-feldspar, quartz, illite, and chlorite. Trace euhedral pyrite is also present.

4.2. Geochronology

Age dating of zircons by U-Pb geochronology by Manaka (2008) yielded an age of 292 ± 3 Ma for a quartz monzonite and an age of 279 ± 4 Ma for the feldspar-phyric dacitic porphyry, indicating that timing of igneous activity at LCT is confined to the Early Permian. In comparison, a sample of rugose coral in Carbonaceous Limestone in the stratigraphically lowest unit returned a fossil age of 360–320 Ma (Cann, 1997; Mason, 1997).

4.3. Structure

Due to deep weathering most of the structural interpretation is derived from orientated structural data. These were collected (8135 readings total) from the majority of diamond drillholes using several different downhole orientation systems. Data are recorded in a dip/azimuth format in degrees.

The stratigraphic sequence is folded on a scale of tens' of meters about very steep generally NNW-plunging (60°/350°) fold axes. The axial plane also dips steeply NNW at the same angles. The folds are chevron (angle ~ 66°) and angular. Centimeter-scale folds are moderately rare (Holcombe, 2012). The dominant bedding orientation dips moderately (55–65°) to the north. The tectonic foliation orientation similarly dips steeply (60–70°) to the north and is very uniform across the deposit. Both bedding and foliation orientations are consistent with regional north directed thrusting (Cairns, 2013).

Two phases of faulting are present at LCT, and these include an older NW striking normal fault set with a moderate to steep (≥45°) SW dip, and a younger NE striking steeply dipping reverse fault set. The NW striking faults are probably related to the Seau Fault, a strike-slip WNW

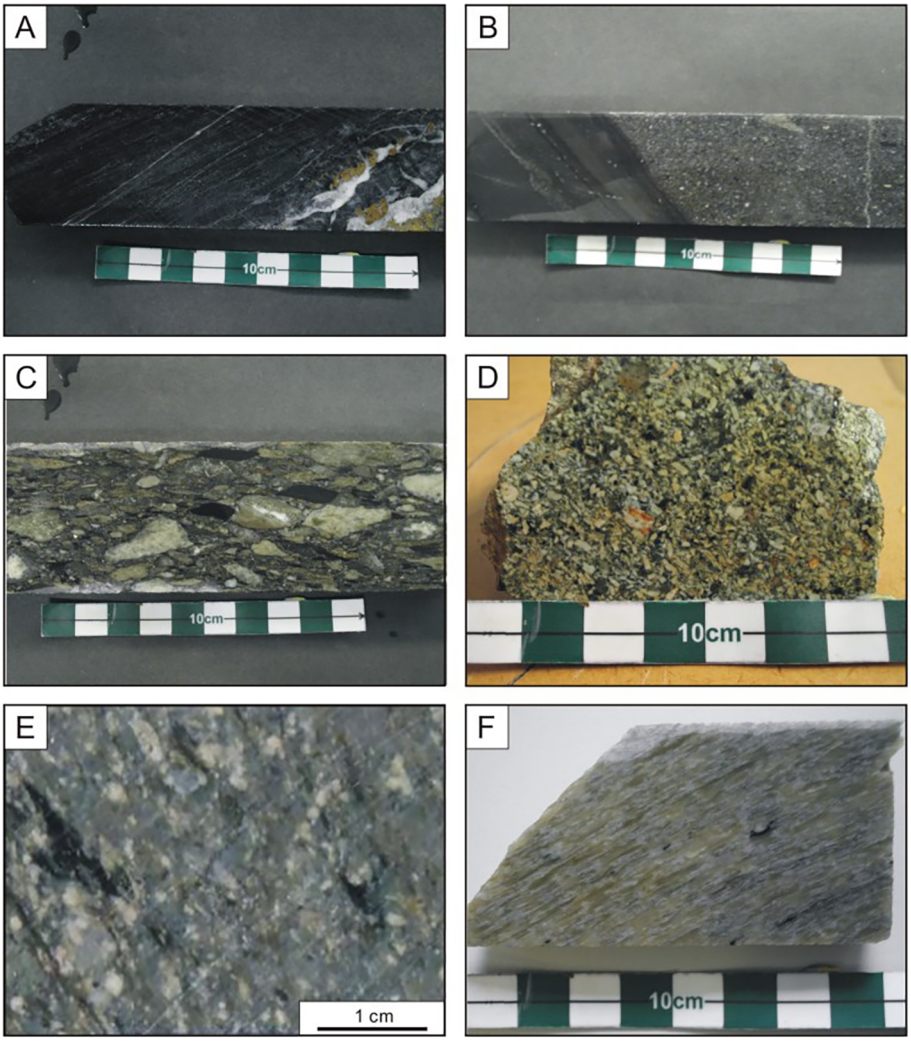

Fig. 6. Representative drillcore and outcrop specimen samples of stratigraphic units at the LCT deposit. A. Limestone enriched in dark carbonaceous materials. Note quartz-sphalerite vein is present in the sample. Sample No. LSD09@88.0m. B. Alternating layers of sandstone and siltstone. Sample No. LSD07@78.0m. C. Sedimentary breccias consisting of polymictic angular to sub-angular clasts. Sample No. LSD24@17.0m. D. Volcaniclastic breccia composing of angular to sub-angular volcanic components. Sample No. LCT-1. E. Lapilli tuff with sparsely distributed small dark green lenticles and altered feldspar grains aligned on a moderately strong foliation. Sample No. LDD006@179.0m. F. Tuffaceous rock with strong sericite-chlorite alteration and strong foliation. Sample No. LSD08@99.3 m. (For interpretation of the references to color in this figure legend, the reader is referred to the web version of this article.)

Table 1
Description of intrusive units of the LCT deposit.

Rock unit	Previous rock name[1]	Age[2]	Occurrence	Composition	Phenocrysts	Groundmass	Distinguishing characteristics
P2	Feldspar-phyric dacitic porphyry	279 ± 4 Ma (Early Permian)	Dikes/stocks, striking NE-SW along fold hinges	Dacite-rhyolite (sub-volcanic)	10–15% tabular plag, 1–3 mm, 5% subhedral qt, < 2 mm, 0–2%, bi books, 0.5–2 mm, 0–2%, euhedral hb, 0.5–2 mm	0.05–1 mm; kf > qt	Majority of mineralized veins hosted within/proximity to this unit
P1b	Quartz monzodiorite	No data	Stocks within the quartz monzonite bodies	Monzodiorite	50–55% tabular plag, 0.5–1 mm, 15–20% euhedral kf, 0.5–1 mm, 15–20% bi books, 0.5–1 mm, 5–10% anhedral qt, 0.1–0.5 mm	No groundmass (equigranular texture)	See below
P1a	Quartz monzonite	292 ± 3 Ma (Early Permian)	Batholith-like bodies, exposing at NE and S end of the deposit	Quartz monzonite	10–15% euhedral kf, 1–10 mm, 5–10% tabular plag, 0.1–5 mm, < 5% bi books, < 5 mm	0.5–1 mm; plag > kf > qt	Stocks of quartz monzonite and quartz monzodiorite cross-cut each other within batholith

Abbreviations; bi = biotite, hb = hornblende, kf = K-feldspar, plag = plagiocalse, qt = quartz; mineral abundances are based on visual estimates of hand specimens and thin sections under microscope.

[1] As used in Manaka (2008).

[2] Ages yielded from LA-ICPMS zircon U-Pb dating in Manaka (2008).

trending fault which is exposed at the south of the deposit. The reverse faults are considered younger than the normal faults as the former occur within the porphyries and the latter transect the sedimentary and volcaniclastic units only. The reverse faults may locally cut veins and has placed the Volcanic Tuff on top of the Undifferentiated Volcaniclastics units.

4.4. Igneous petrochemistry

Whole rock geochemical composition of the freshest available representative samples from the intrusive rock types are presented in Table 2. Quartz monzonite and quartz monzodiorite units are grouped together in this section as field evidence suggests that they are co-magmatic. All feldspar-phyric dacitic porphyry samples are altered to some extent, and thus whole rock geochemical compositions of the samples were plotted on tectonic discrimination diagrams to investigate the likely regional tectonic setting of magmatism.

The AFM ternary diagram in Fig. 8A shows the LCT intrusive units are classified into the calc-alkaline series (except for one quartz monzonite sample). Discrimination diagrams using less mobile elements such as Nb/Y vs Zr/TiO_2 show that the LCT samples display mostly within the rhyolite/dacite fields (Fig. 8B), which are comparable to the lithological descriptions assigned from hand specimens and petrography. On the tectonic discrimination diagram for granitic rocks the quartz monzonite/quartz monzodiorite samples plot in the volcanic-arc field, whereas the majority of feldspar-phyric dacitic porphyry samples lie in the volcanic-arc field and in the syn-collisional field near the boundary with the volcanic-arc field (Fig. 8C).

The chondrite-normalized rare earth elements (REE) patterns of the quartz monzonite/quartz monzodiorite units are characterized by flat to steep dipping patterns with a distinctive negative Eu anomaly (Fig. 9). Such REE patterns are regarded as a typical signature of a highly fractionated magma (e.g., Wilson, 1989). The REE patterns of the feldspar-phyric dacitic porphyry show enriched Light REE (LREE) and are flat in the Middle REE (MREE) to Heavy REE (HREE), with moderate dips from LREE to HREE and a negligible Eu anomaly (Fig. 9). These characteristics are typically recognized as features of fertile suites which are commonly associated with porphyry mineralization (Loucks, 2014).

5. Mineralization, alteration and paragenesis

Mineralization characteristics of the LCT deposit are described below and the paragenesis of veins and alteration is summarized in Fig. 10.

5.1. Veining

Mineralization at LCT occurs predominantly within veins which are present in almost all lithologies. The highest concentrations of veins occur at the contact zones between the intrusions and other lithologies. Individual veins may extend both laterally and vertically for several tens of meters. Vein thickness commonly ranges from hairline to several tens of centimeters. The veins are classified into four main types based on texture and mineral assemblage, including quartz-carbonate undifferentiated (VNN), base metal (BMV), massive pyrite (MPY) and buck (BUK) vein types. All of the vein types except BUK veins are mineralized and the frequency of vein occurrence is spatially associated with the feldspar-phyric deictic porphyry intrusions/dykes.

5.1.1. Quartz-carbonate undifferentiated (VNN) veins

These veins commonly occur in the upper and lower mineralized zone within and immediately adjacent to the dacitic porphyry dykes. They usually consist of quartz veins which often appear as regionally deformed, wispy to thick irregular stockworks (Fig. 11A). The veins were infiltrated by carbonate, pyrite, sphalerite, galena, chalcopyrite

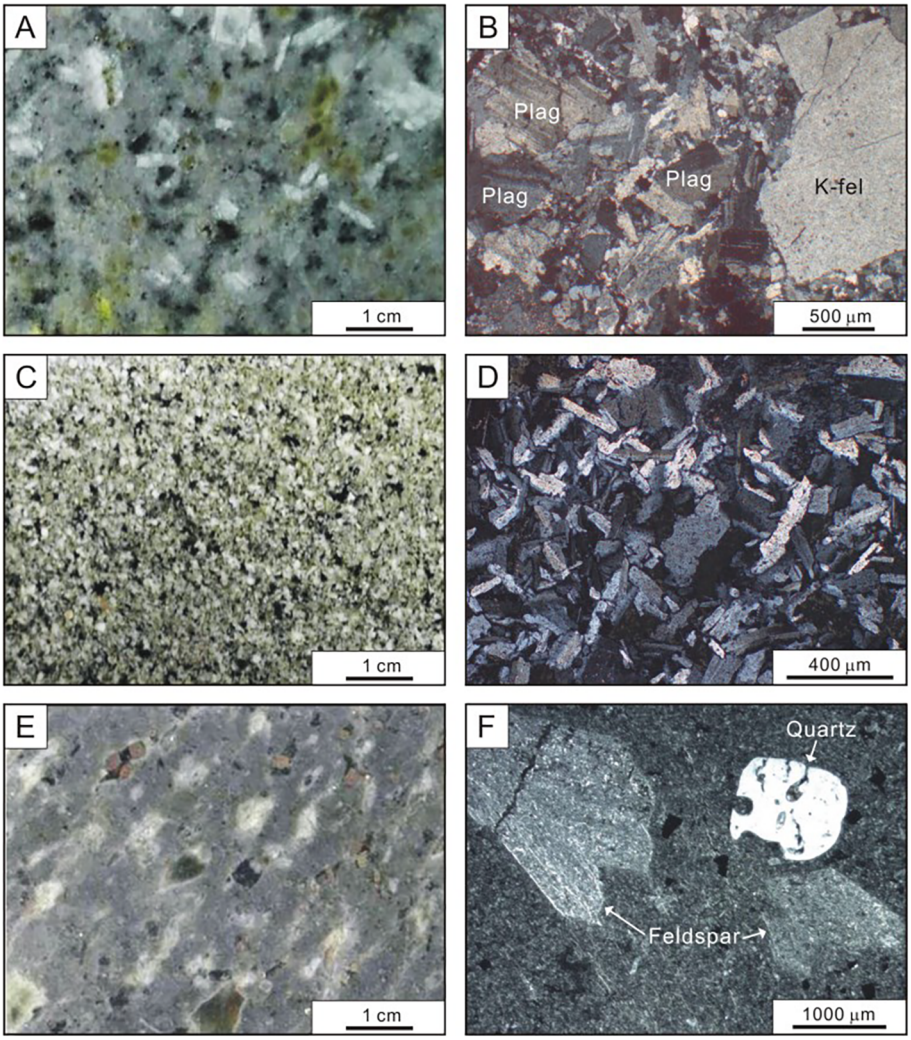

Fig. 7. Representative sectioned drillcore specimen samples and thin sections of intrusive units at the LCT deposit. A. Photograph showing a hand specimen sample of quartz monzonite. Sample No. LSD18@70.7m. B. Photomicrograph showing K-feldspar and plagioclase phenocrysts in finer-grained groundmass. Sample No. LSD18@70.7m. C. Photograph showing a hand specimen sample of quartz monzodiorite. Sample No. LSD15@99.1m. D. Photomicrograph showing plagioclase-dominated equigranular texture of quartz monzodiorite. Sample No. LSD15@99.1m. E. Photograph showing a hand specimen sample of feldspar-phyric dacitic porphyry. Sample No. LDD234@216.3m. F. Photomicrograph showing embayed quartz phenocrysts (right) and sericitized feldspar phenocrysts in devitrified quartzo-feldspathic groundmass. Sample No. LDD234@216.3m. Abbreviations; K-fel = K-feldspar, Plag = plagioclase.

and chlorite (Fig. 11A). They may contain trace amounts of arsenopyrite and molybdenite. The VNN veins commonly display crustiform/colloform textures (Fig. 11B).

5.1.2. Base metal (BMV) veins

These veins are characterized by deformed aggregates of sphalerite and galena which typically occupy the vein centers with traces of other sulfides such as pyrite and chalcopyrite (Fig. 11C and D). BMV veins have a similar mineral assemblage as VNN veins but contain significantly more base metal sulfides. Sphalerite is usually the dominant mineral with lesser galena and pyrite. Both the BMV and VNN veins contain free gold grains which are usually microscopically identified.

5.1.3. Massive pyrite (MPY) veins

These occur as irregular tightly packed fine- to coarse-grained pyrite ± chalcopyrite intergrowths (Fig. 11E). The MPY veins often overprint or cross-cut VNN veins (Fig. 11F). Significant gold mineralization is rare in this vein type although Cu grades may range up to several percent. Pyrite veinlets are mineralogically similar to MPY veins and usually occur as stringers (≤ 0.5 cm). They may also contain trace chalcopyrite and gangue minerals such as quartz, carbonate and chlorite.

5.1.4. Buck (BUK) veins

The veins commonly occur as moderate to thick veins (up to 20 cm) consisting of massive coarse crystalline quartz with chlorite and minor carbonate. BUK veins are sometimes misclassified with VNN veins due to the presence of minor to trace sulfides but are distinguished from VNN veins by their milky quartz composition, massive to weakly deformed appearance and barren to minor sulfide content. They do not contain significant gold grades and are considered to be post-mineralization metamorphogenic veins associated with lower greenschist facies metamorphism.

5.2. Vein structure

The majority of the mineralized veins are hosted within and adjacent to the feldspar-phyric dacitic porphyry intrusions/dykes. Structural measurements in oriented drillcore identified three distinct prominent sets of vein orientations including steep NNE dipping veins (66°/010°), steep NNW dipping veins (70°/340°) and gentle to moderate SSE dipping veins (21°/172°) (Fig. 12A). The two former orientations are measured in all types of veins, whereas the latter orientation is found only in VNN and BUK veins (Fig. 12B).

Significant gold grades are associated with base metals (Pb, Zn, Cu) and are predominantly hosted in the steep NNE dipping veins. Minor gold with high Cu and Zn grades also occurs in the steep NNW dipping veins (Fig. 12C–F). In contrast, the gentle to moderate SSE dipping VNN veins are elevated in gold with moderate Zn and Pb grades (Fig. 12C, E and F).

These structural measurements indicate that the earliest VNN veins are probably controlled by the moderate south dipping fault and this structure is also related to the formation of late stage south dipping BUK veins which may have cross-cut and re-opened the earlier VNN veins.

Table 2
Whole rock geochemistry of igneous units of the LCT deposit.

Sample No.	227,272 mE	LSD08-76.9	LSD08-83.7	LSD15-97.3	LSD16-99.2	LSD16-101.0	LSD16-107.1	LSD04-87.2	LSD03A-65.1	LDD81-81.5	LDD81-67.7	LDD81-58.5	LRD67-64.0	LSD09-50
Rock Type	QMZ/MZD	QMZ/MZD	QMZ/MZD	QMZ/MZD	QMZ/MZD	QMZ/MZD	QMZ/MZD	FPDP	FPDP	FPDP	FPDP	FPDP	FPDP	FPDP
Major elements (%)														
SiO_2	66.24	67.33	65.29	70.26	65.33	65.42	66.06	68.82	71.50	75.92	75.48	72.57	74.17	70.31
TiO_2	0.71	0.26	0.22	0.17	0.3	0.27	0.25	0.18	0.17	0.16	0.16	0.17	0.17	0.28
Al_2O_3	17.61	15.64	13.30	15.05	16.08	15.60	15.72	14.57	13.00	12.52	12.51	14.32	12.84	12.81
Fe_2O_3	2.85	3.35	6.01	2.65	3.75	3.43	3.37	2.23	1.98	0.23	0.59	0.42	1.19	4.08
MnO	0.02	0.05	0.04	0.05	0.03	0.03	0.04	0.02	0.01	< 0.01	< 0.01	< 0.01	0.01	0.04
MgO	1.99	0.83	0.55	0.81	1.07	0.82	0.89	0.39	0.14	0.15	0.14	0.19	0.24	0.85
CaO	0.46	1.38	1.64	0.72	2.04	2.34	1.47	0.06	< 0.01	< 0.01	< 0.01	< 0.01	< 0.01	0.39
Na_2O	3.59	6.00	6.44	7.70	4.56	4.57	4.61	0.17	0.08	0.15	0.16	0.17	0.22	6.15
K_2O	2.27	1.67	0.79	0.35	5.22	5.08	5.47	11.47	9.72	9.87	10.1	10.98	10.18	0.55
P_2O_5	0.18	0.10	0.10	0.06	0.12	0.10	0.11	0.08	0.05	0.07	0.06	0.07	0.05	0.09
LOI	2.88	3.21	4.99	1.74	1.26	2.08	1.67	1.36	1.87	0.61	0.61	0.85	0.94	2.63
Total	98.83	99.85	99.41	99.56	99.75	99.74	99.67	99.77	99.50	100.09	100.20	100.20	100.46	99.54
S	0.4	1.90	4.64	0.99	< 0.01	0.01	0.01	1.08	1.34	0.01	< 0.01	< 0.01	0.11	2.15
Trace elements (ppm)														
Y	15	24	27	28	24	25	23	12	8	10	9	10	7	< 1.5
U	7	15	9	16	13	15	15	3	3	4	4	4	4	18
Rb	129	76	34	12	175	160	181	260	219	215	220	235	232	106
Th	30	50	39	54	46	50	47	13	16	12	13	14	13	102
Pb	10	13	47	10	15	16	13	192	3500	850	696	928	954	5
As	51	1236	80	20	7	10	5	21	177	22	17	17	309	74
Bi	< 2	2	5	< 2	< 2	< 2	< 2	< 2	< 2	< 2	< 2	< 2	< 2	5
Zn	26	31	23	38	23	37	35	93	1440	17	22	19	115	66
Cu	6	22	355	27	13	6	25	12	96	6	8	8	7	30
Ni	2	3	3	1	5	4	4	3	2	2	3	2	2	53
Sn	10	4	3					< 2	< 2	< 2	< 2	< 2	< 2	18
Nb	24	20	12	22	18	19	19	6	7	6	6	6	6	8
Zr	277	329	247	317	291	316	308	137	139	126	127	145	136	6
Sr	116	139	148	165	446	381	242	61	41	41	47	54	64	24
Cr	1	3	3	75	64	54	61	1	< 1	< 1	< 1	< 1	< 1	24
Ba	220	155	79	41	632	568	609	3304	3907	3020	3032	3415	2833	24
Sc	21	6	4	5	8	7	6	2	< 2	< 2	2	2	1	23
V	134	39	32	17	49	36	39	46	16	11	12	16	17	< 2
La	< 2	56	34	45	53	73	129	19	19	20	23	23	18	60
Ce	7	92	66	92	88	118	162	38		39	42	46	38	29
Nd	4	36	25	35	33	38	43	11	16	13	14	15	12	4
La	3	60.6	36.9							20.1		23.0	19.1	
Ce	7.40	113.8	69.9							35.0		40.3	32.9	
Pr	1.03	12.12	7.82							3.57		4.04	3.32	
Nd	4.66	42.3	28.3							12.2		13.5	11.2	
Sm	1.20	7.14	5.30							1.94		2.12	1.57	
Eu	0.19	0.85	0.59							0.70		0.65	0.50	
Gd	1.52	5.31	4.69							1.52		1.66	1.21	
Tb	0.30	0.80	0.82							0.22		0.24	0.18	
Dy	2.13	4.65	4.98							1.37		1.49	1.06	
Ho	0.49	0.94	0.99							0.30		0.31	0.22	
Er	1.55	2.79	3.00							0.98		1.04	0.74	
Tm	0.25	0.43	0.46							0.16		0.17	0.12	
Yb	1.77	2.91	3.00							1.18		1.22	0.93	
Lu	0.30	0.45	0.45							0.20		0.21	0.16	

Abbreviations; FPDP = feldspar-phyric dacitic porphry, QMZ = quartz monzonite, MZD = Quartz monzodiorte. Samples were analyzed for major (Si, Ti, Al, Fe, Mn, Mg, Ca, Na, K and P) and trace (Rb, Sr, Ba, Sc, V, Cr, Ni, Zn, Y, Zr, Nb and Pb) elements using the X-ray Fluorescence (XRF) at CODES, the University of Tasmania. Rare earth elements (REE: La, Ce, Pr, Nd, Sm, Eu, Gd, Tb, Dy, Ho, Er, Tm, Yb and Lu) of 12 of these samples were also analyzed using the solution ICP-MS at the University of Tasmania.

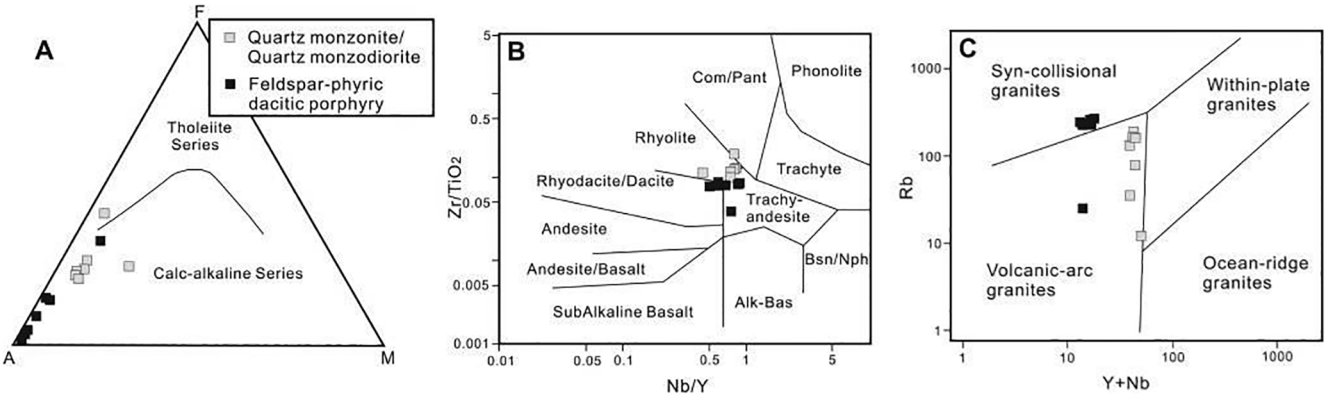

Fig. 8. Geochemical discrimination diagrams for the igneous units of the LCT deposit. A. AFM ternary diagram (after Irvine and Bargar, 1971). A = Na_2O + K_2O, F = total FeO, M = MgO. B. Nb/Y vs Zr/TiO_2 classification diagram (after Winchester and Floyd, 1977). C. Y + Nb vs Rb discrimination diagram for felsic rocks (after Pearce et al., 1984).

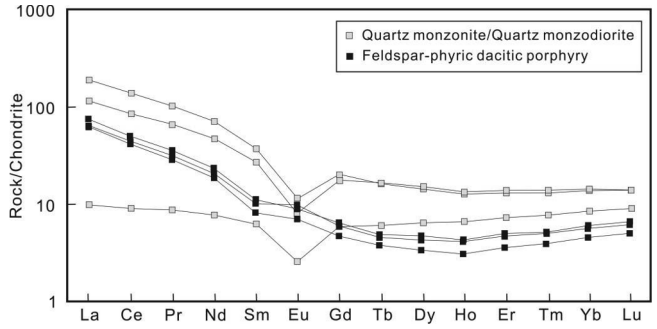

Fig. 9. Chondrite-normalized REE patterns of the igneous rock units of the LCT deposit. Normalized values of Sun and McDonough (1989) were applied.

The steep NNE and NNW dipping vein sets enriched in base metals are considered to be of the same generation (Libao, 2015).

5.3. Gold mineralization

The highest gold grades occur within the feldspar-phyric dacitic porphyry intrusive body and at the contact with the surrounding country rocks of volcanogenic units. This mainly reflects the more intense fracturing and veining at the contact zones. High grade Pb and Zn values exhibit similar characteristics. Higher metal grades generally decline towards the north of the deposit.

The distribution of moderate to high gold grades is generally highly variable. Gold principally occurs in the veins as previously described, but minor gold mineralization also occurs in the matrix of the polymictic sedimentary breccia, where the organic carbon in the breccia matrix may have acted as a reducing or adsorption agent to precipitate gold from the fluids. Gold occurs mineralogically as electrum and native gold, frequently in association with pyrite, but also occurs together

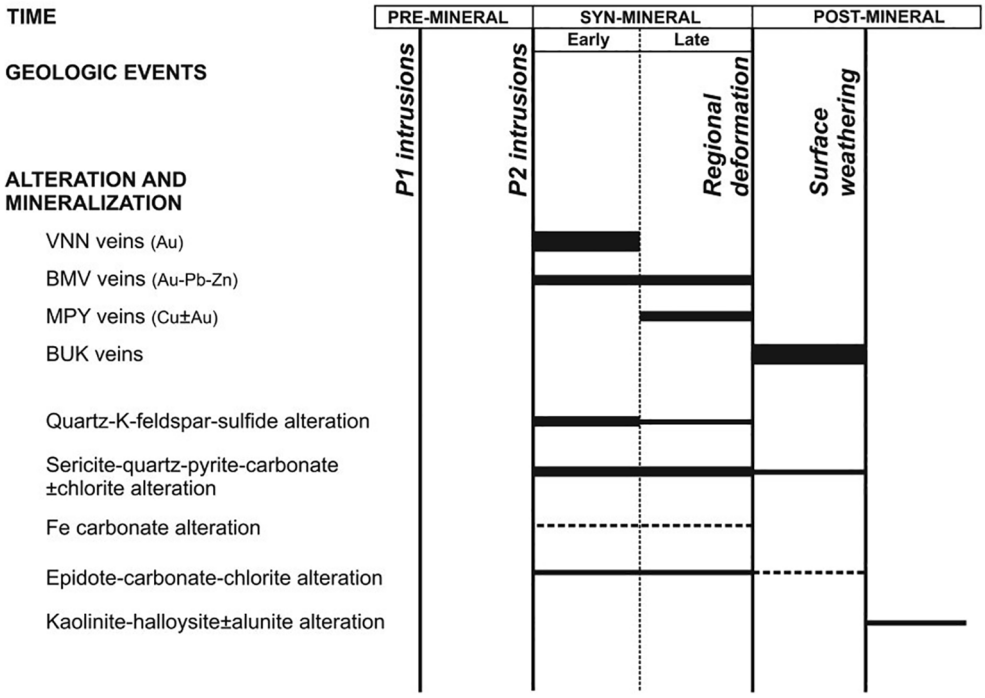

Fig. 10. Paragenetic diagram illustrating the timing relationships of alteration and mineralization. Widths of bars indicate the approximate intensity of events. Relationships between stages were determined by cross-cutting and overprinting contacts in field and petrography studies.

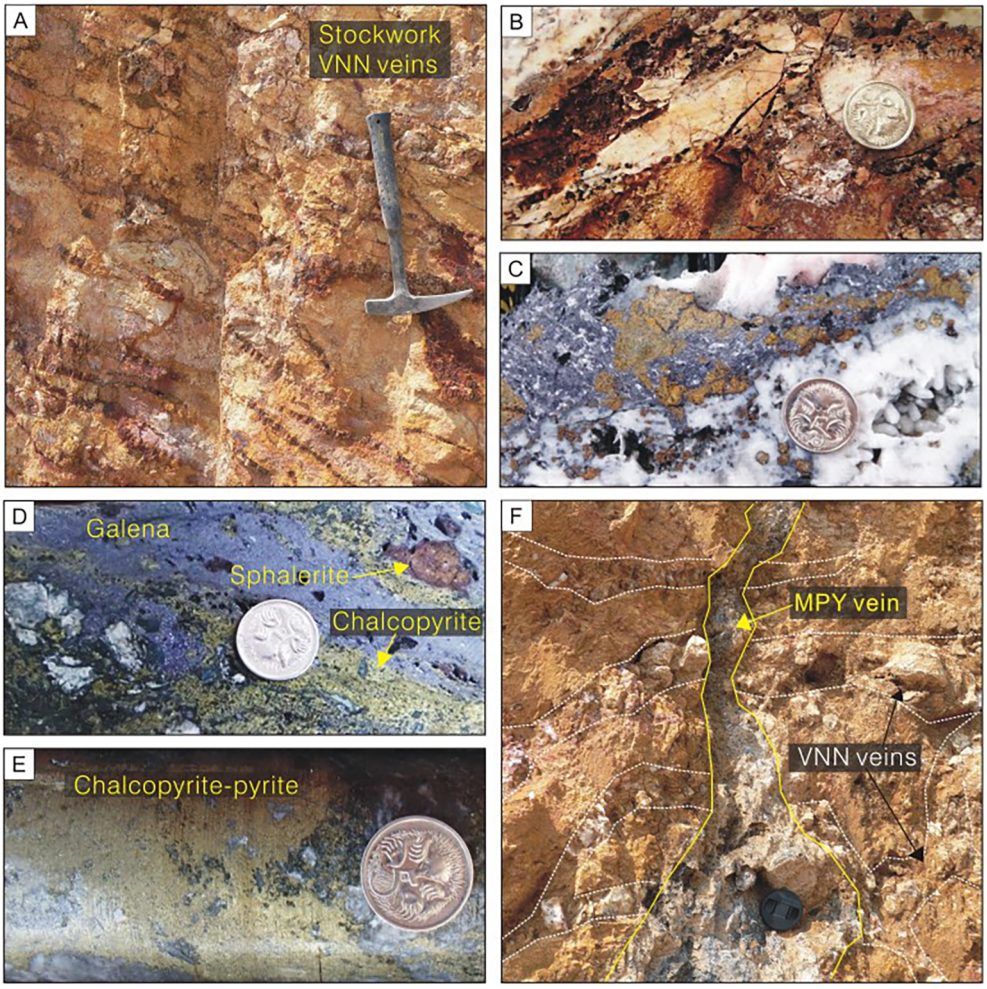

Fig. 11. Characteristics of mineralized veins at the LCT deposit. A. Mineralized VNN veins at surface exposure showing sub-parallel NW-SE orientation Note the veins are oxidized with hematite (red) along the vein margins. B. Typical VNN veins exposed at surface. Note that the veins are commonly oxidized and characterized by gossanous cavities. C. The sample contains 1.30 g/t Au, 45.3 g/t Ag, 23.1% Pb, and 17.5% Zn within a dense quartz-sphalerite-galena BMV vein. Sample No. LDD034@103-104m. D. BMV vein consisting of pyrite, quartz, chalcopyrite, galena and minor sphalerite. Analyses include 0.67 g/t Au 18.6 g/t Ag, 0.63% Cu, 0.13% Pb and 0.31% Zn. Sample No. LDD010@225.3m. E. MPY vein of massive chalcopyrite and pyrite sulfides. F. Vein exposure showing earlier VNN stockwork (outlined by dashed white) veins cross-cut and overprinted by later MPY vein (outlined by yellow). Black camera lens at bottom is for scale. (For interpretation of the references to color in this figure legend, the reader is referred to the web version of this article.)

with chalcopyrite, sphalerite, galena, arsenopyrite and molybdenite. The electrum commonly occurs as inclusions in the vein-hosted pyrite, but is also occasionally found as free grains in the veins ranging from < 10 to 100 μm in size (Fig. 13A and B). The gold fineness of the electrum was determined by microprobe analysis and demonstrated a range of 520–870 (n = 5), indicating that some (above 800) can be compositionally classified as native gold (Manaka, 2008).

5.4. Alteration

Five distinct alteration assemblages are recognized at the LCT deposit. They are described below in order generally ranging from the deposit center to the periphery.

5.4.1. Quartz-adularia-sulfide

This mineral assemblage is developed exclusively within the dacitic porphyry intrusions/dykes. In hand specimen, rocks which have undergone this alteration are hard and grey in colour due to intense silicification (Fig. 14A). K-feldspar is difficult to identify in hand specimen but petrography (Mason, 1997) and chemical staining confirm that fine-grained adularia is pervasively present in the rocks (Fig. 14B). Disseminated pyrite (0.5–1%) is commonly present with this alteration phase. Petrographic examination indicated that some plagioclase phenocrysts are replaced by quartz, but the groundmass and most other minerals are converted to adularia.

5.4.2. Sericite-quartz-pyrite-carbonate ± chlorite

In areas with abundant mineralized stockwork veins the host porphyry intrusions/dykes and immediately adjacent host sequence are commonly affected by sericite-quartz-pyrite-carbonate with localized chlorite alteration (Fig. 14C). The alteration assemblage is most prominent along fractures and vein selvages. In addition, sericite has been observed to preferentially alter particular beds and clasts within the volcanogenic sediments. Pyrite is typically fine-grained and uniformly disseminated as single grains or fine aggregates. Silica alteration is most intense throughout the mineralized porphyry rock and the adjacent volcanic and breccia zones. Within most drillholes it is observed that the onset of increased silica alteration corresponds to the appearance and increase in sulfides. This assemblage generally grades into barren sericite-quartz-chlorite in the volcanics/volcaniclastics units.

Some sericite-rich parts of this alteration style are overprinted by the foliation and are unrelated to the mineralization event and show no clear spatial relationship with the dacitic porphyry dykes. Crawford (2013) suggested that such sericite alteration is potentially a result of low-grade burial metamorphism rather than hydrothermal processes associated with intrusive derived fluids. One possible cause of increased sericite alteration is attributable to regional deformation.

5.4.3. Fe carbonate

This alteration locally occurs in the Volcanic Tuff unit immediately adjacent to the dacitic porphyry dykes. The Fe carbonate minerals include ferroan-calcite and siderite which selectively replace feldspars. It is difficult to recognize this alteration in fresh samples, but in drill cores and outcrops which have been exposed to air for several months it becomes apparent as pronounced brown stains (Fig. 14D).

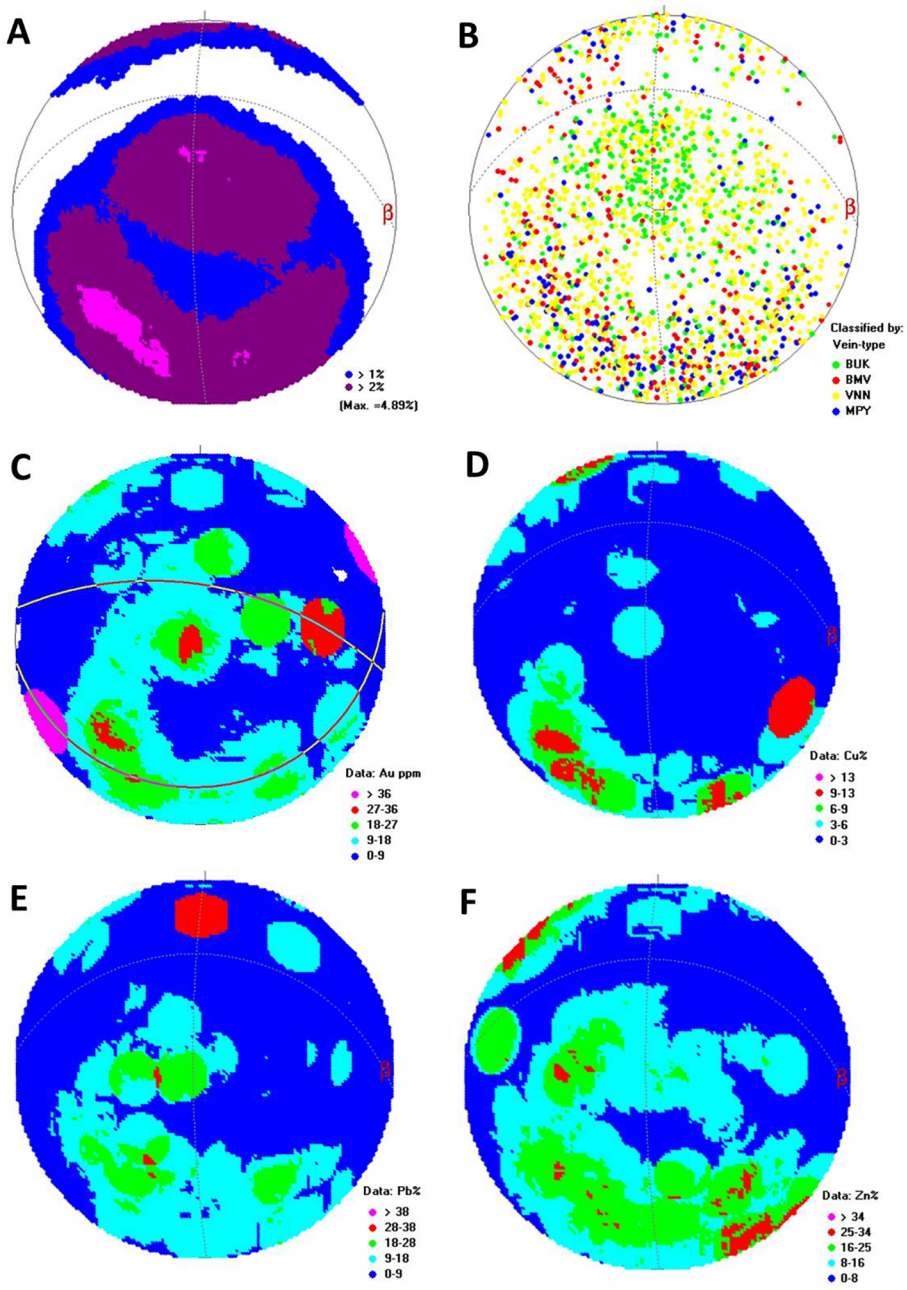

Fig. 12. A. Plot of vein frequency with three distinct populations showing two dominant vein sets of steep NNE and NNW dipping vein orientations and east –west striking moderately south dipping set. B. Plot of vein frequency based on differentiated vein types. C. Plot of cumulative Au values shows that the gold-bearing veins have a variety of orientations but the dominant vein set dips steeply to the northeast and the south-dipping veins also contain some high gold values. The anomalous gold value (pink circle) located at the low frequency part of the plot corresponds to a single BMV vein which returned 176 g/t Au. D. Plot of cumulative Cu values shows that most of the veins yielding high copper values dip steeply to the NNE or NNW. E and F. Plots of Pb and Zn respectively show similar frequency distribution and they correspond to all of the recognized vein orientations. (For interpretation of the references to color in this figure legend, the reader is referred to the web version of this article.)

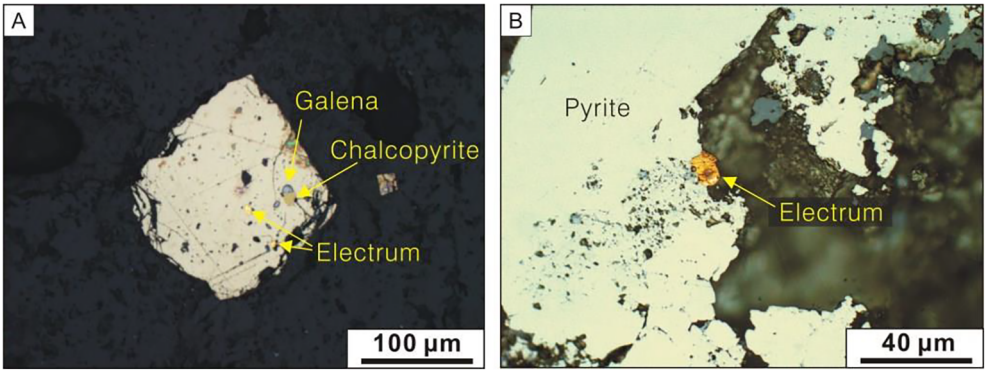

Fig. 13. Gold occurrence of the LCT deposit. A. Electrum, galena and chalcopyrite inclusions in pyrite. Sample No. LDD03A@50.7m. B. Free electrum grain enclosed by pyrite. Sample No. LRD67@43.0m.

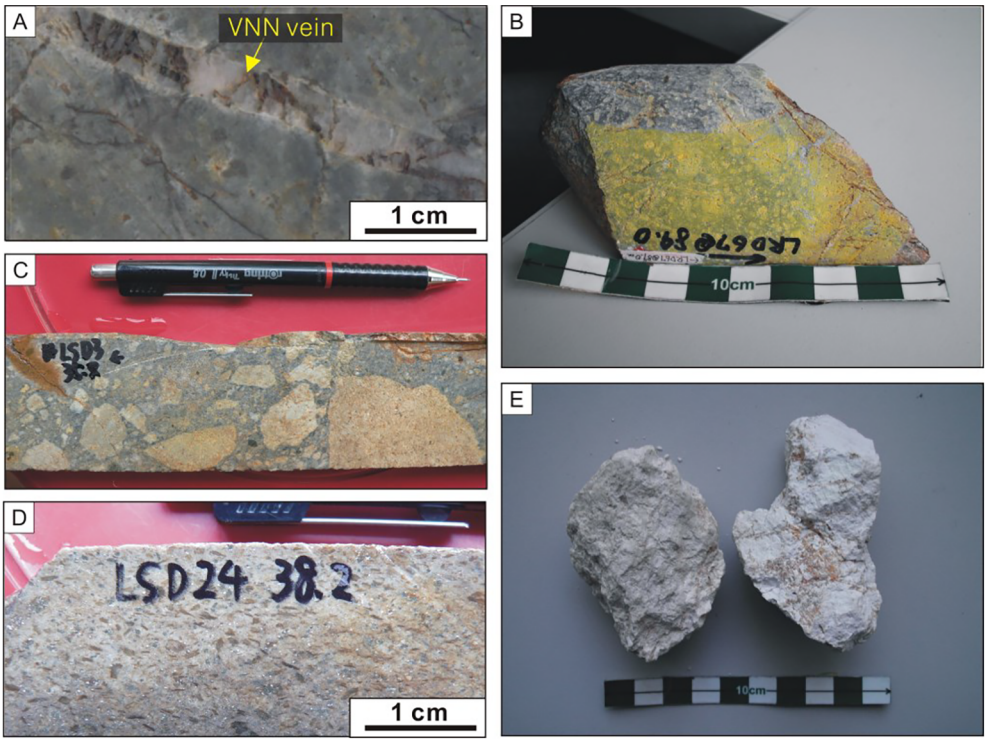

Fig. 14. Characteristics of alteration phases recognized at the LCT deposit. A. Feldspar-phyric dacitic porphyry intrusion sample altered by quartz-K-feldspar-sulfides assemblage with VNN vein. Note intense silicification is developed in the sample. Sample No. LDD38@96.7m. B. Positive result of K-feldspar staining (yellow) in the silicified feldspar-phyric dacitic porhyry. Sample No. LRD67@89.0m. C. Sedimentary breccia sample showing clasts are selectively altered by sericite and the matrix is altered by fine-grained quartz-pyrite-carbonate minerals. Sample No. LSD03@35.7m. D. Phenocrysts of Volcanic Tuff sample are selectively replaced by Fe carbonates and are now stained to brown. Sample No. LSD24@38.2m. E. Samples collected from surface are intensely altered to Kaolinite-halloysite ± alunite assemblage. (For interpretation of the references to color in this figure legend, the reader is referred to the web version of this article.)

5.4.4. Epidote-carbonate-chlorite

Most of the volcaniclastic sediments and P1a, P1b and P2 intrusive units are affected by weak pervasive propylitic alteration consisting of an epidote-carbonate-chlorite assemblage (Fig. 6F). This facies is interpreted to form a distal halo to the mineralization. Mafic silicates are converted to chlorite and magnetite is converted to pyrite (usually less than 1%). Feldspars are partially converted to sericite or albite in some intrusive rocks. Minor epidote may replace calcic plagioclase. In some volcaniclastic sandstones, oxidation of chlorite produces a distinctive reddish pink color in weathered outcrops. Similar mineral assemblages may also represent regional propylitic alteration.

5.4.5. Kaolinite-halloysite ± alunite

The latest stage alteration is represented by kaolinite and halloysite with minor alunite (Fig. 14E). This mineral assemblage commonly overprints all earlier mineralization stages and alteration facies and is interpreted to be the result of a combination of steam-heated hot spring alteration and weathering and oxidation under acidic oxidizing conditions. It is thickest in the central zone of the deposit area where the stockwork veins are mainly developed and forms a blanket-like cover up to 100 m thick. In comparison this alteration is only a few tens of meters deep in other parts of the deposit. Kaolinite and halloysite are the dominant minerals and are typically white or yellow in colour. The primary rock texture is usually completely destroyed. Secondary alunite is locally developed and mostly occurs as infill of the earlier stage vein cavities.

6. Discussion

6.1. Regional tectonic setting

The LCT deposit occurs within a regionally extensive pluto-volcanic suite of Late Carboniferous-Early Permian age (310–275 Ma; Meffre et al., 2011) of the TSFB, which regionally hosts epithermal style Au-Ag mineralization at Ban Houayxai (Manaka et al., 2014), and the Phu Kham porphyry-related skarn Cu-Au deposit (Kamvong, 2013) in the MEPA concession area. Geological field relationships at LCT suggest that the formation of the mineralized stockwork veins occurred immediately after the emplacement of the dacitic porphyry intrusion in the Early Permian (c.a. 280 Ma). In the context of regional tectonics this timing corresponds to the late stage magmatic events of the TSFB formed by southward subduction of oceanic crust beneath the Indochina Terrane (Meffre et al., 2011; Fig. 8A and B). This is supported by whole rock geochemical data, as the dacitic porphyry intrusions plot in both the volcanic-arc and syn-collisional fields (Fig. 8C). This may indicate that the magma responsible for the intrusions contained a higher crustal component compared to the earlier quartz monzonite and quartz monzodiorite intrusions. Timing of the regional metamorphism along the TSFB is confined to 270–230 Ma (e.g., Nakano et al., 2007), and thus is consistent with the interpreted tectonic setting responsible for the dacitic porphyry intrusions at LCT. Therefore, these geological data suggest that the mineralizing event at LCT is genetically linked to the magmas associated with the regional subduction-collision event of the Early Permian.

6.2. Deposit model

A model for the LCT deposit is proposed principally from the geological studies described in this paper (Fig. 15). The structural setting at LCT is moderately complex as suggested by multiple mineralized vein types and timing. Structural data indicate that the dacitic porphyries were intruded during the transition between structural regimes as evidenced by later reverse faults which are observed only in the intrusive bodies. Thus, this may suggest that the mineralizing event occurred in a transitional environment from extensional to compressional stress regimes.

The vein-hosted mineralization is concentrated at the contact zone and margins of the subvolcanic stocks intruded into the volcanosedimentary sequence, implying that the stocks acted as the heat source and provided the bulk of the metals in magmatic fluids.

The minimum depth of formation of mineralization at LCT is estimated to be at least1 km below surface based on the field association of mineralization with the sub-volcanic intrusive rocks (i.e., dacitic porphyry intrusions). The close association of the intrusions with the veins,

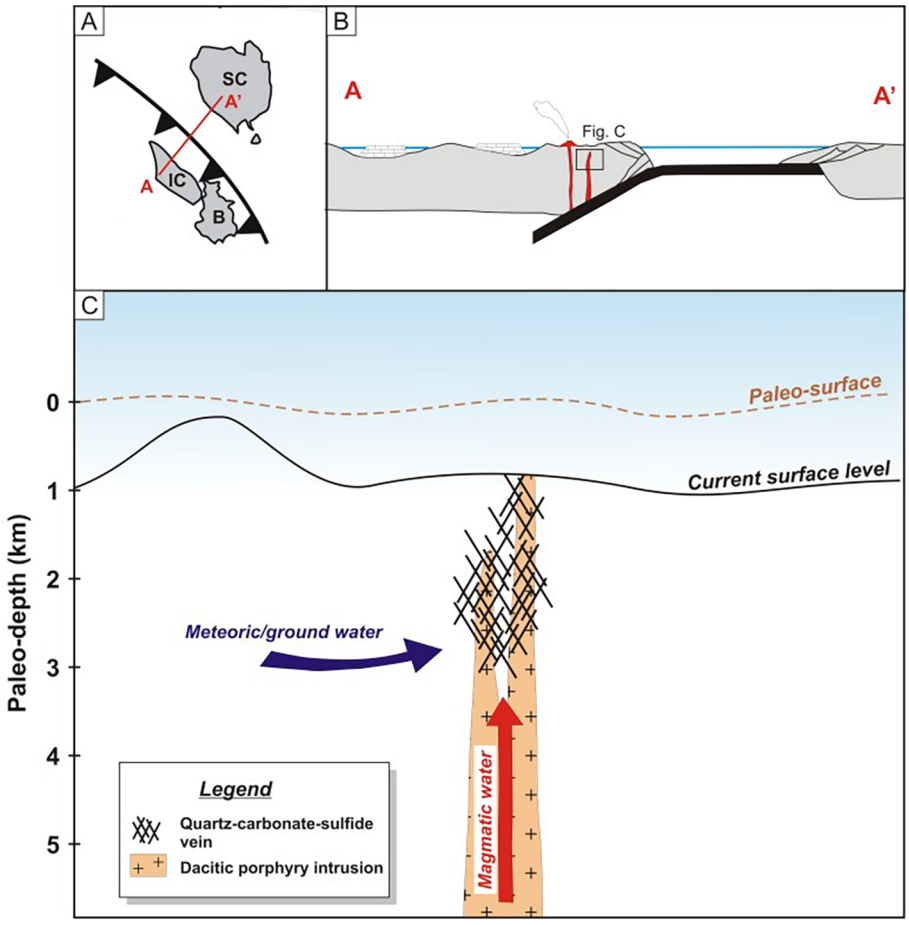

Fig. 15. Reconstructed tectonic and deposit model for the LCT deposit. A and B. Reconstructed tectonic setting of the Indochina Terrane and the surroundings during Early Permian (280–270 Ma), showing magmatism along the TSFB occurs as a result of subduction of the South China oceanic plate beneath the Indochina plate. Model is modified after Shi et al. (2015). C. Proposed genetic model for the LCT deposit. Abbreviations; SC = South China, IC = Indochina, B = Borneo.

and their porphyritic texture and intermediate grain size indicate a level of emplacement of greater than 2 km depth. This suggests a subvolcanic origin for the LCT deposit. In comparison epithermal deposits typically form at depths of less than 1 km from surface (Hedenquist et al., 2000). The presence of kaolinite-halloysite ± alunite alteration most likely formed by steam heated hot spring activity suggests there was ongoing relatively rapid uplift and unroofing of the system, commensurate with the contemporary tectonic activity of the TSFB (Fig. 15).

These geological conditions suggest that fluid mixing is likely to be the principal ore precipitation mechanism at LCT, where mixing of the magmatic ore fluids with cooler and less saline meteoric water resulted in cooling, dilution, neutralization and precipitation.

7. Conclusions

The Early Permian dacitic porphyry intrusions are shown to be genetically linked to the mineralizing event at LCT and are a part of magmatic units of TSFB. The magmas responsible for the intrusions are considered to have resulted from the regional subduction-collision event of the Indochina and South China Terranes during the Early Permian.

The Au-Ag-Cu-Pb-Zn mineralization at the LCT deposit occurs as stockwork veins hosted in and adjacent to dacitic porphyry intrusions in Early Permian age. Mineralization is considered to have formed at depths of 1–3 km from surface and the deposit is subsequently described as subvolcanic in style.

Acknowledgements

Numerous geologists and consultants have over the years of exploration added to the data base and contributed their knowledge and ideas to the understanding of this unusual deposit. This paper is the result of a synthesis and review both of this exploration database and the research data collected by Takayuki Manaka during the course of his M.Sc. thesis. Much of our understanding of the regional metallogenesis came from discussions with Professor Khin Zaw of the University of Tasmania, and of the regional geology with Cameron Cairns. The drilling program completed in 2012-2013 owes much of its operational success to the efforts of Ben Tucker and Steve Farmer who led the dedicated multicultural team of geologists and geotechnicians during this intensive exploration phase, including Evelyn Abaño, Efren Pariña and Nick Primaleon. Thanks are also due to Roselynne Petate for drafting many of the figures. The draft paper was significantly improved by comments offered by Imants Kavalieris. The authors wish to thank Phu Bia Mining and PanAust for permission to publish this paper. Lastly and most importantly, this paper is dedicated to Khonesavanh Sisouphanh and Sompheng Masodsai who lost their lives at LCT on 2nd June 2014.

Appendix A. Supplementary data

Supplementary data to this article can be found online at https://doi.org/10.1016/j.oregeorev.2019.02.010.

References

Backhouse, D.J., 2004. Geological setting, alteration and nature of mineralization at the Phu Kham Copper-Gold Deposit Laos PDR. Unpublished B.Sc. (Honors) thesis. CODES, University of Tasmania, pp. 141.

Black, L.P., Kamo, S.L., Allen, C.M., Aleinikoff, J.N., Davis, D.W., Korsch, R.J., Foudoulis, C., 2003. TEMORA 1; a new zircon standard for Phanerozoic U-Pb geochronology. Chem. Geol. 200, 155–170.

British Geological Survey, 1990. Lao PDR geological and mineral occurrences map on scale 1:1,000,000.

Cairns, C., 2013. PBM Contract Area Regional Geological Map Update. Phu Bia Mining, Vientiane.

Cann, J., 1997. In: "Memorandum Re: Thin Section of Coral" Appendix 2 in Mason, D., Petrographic Descriptions and Interpretation for Twenty Drill core Rock Samples, Long Chieng Track Prospect (Lao PDR)". Mason Geoscience Pty Ltd Report for Phu Bia Mining Ltd, pp. 17.

Carter, A., Clift, P.D., 2008. Was the Indosinian orogeny a Triassic mountain building or a thermotectonic reactivation event? C. R. Geosci. 340, 83–93.

CODES-Industry Project, 2014. Ore Deposits of SE Asia 2011–2014. Centre for Ore Deposit Research (CODES), University of Tasmania.

Corfu, F., Hanchar, J.M., Hoskin, P.W.O., Kinny, P.D., 2003. Atlas of zircon textures. Rev. Mineral. Geochem. 53, 469–500.

Crawford, A.J., 2013. Petrographic report on 25 rocks from the Long Chieng deposit, Lao PDR. Unpublished external consultant report. Crawford Geological Research Consultants, pp. 104.

Cromie, P.W., 2010. Geological setting, geochemistry and genesis of the Sepon gold and copper deposits, Laos. Unpublished Ph.D thesis. CODES, The University of Tasmania, Hobart, Tasmania, pp. 395.

Cromie, P.W., Makoundi, C., Zaw, Khin, Cooke, D.R., White, N., Ryan, C., 2018. Geochemistry of Au-bearing pyrite from the Sepon Mineral District, Laos PDR, Southeast Asia: implications for Ore Genesis. J. Asian Earth Sci. 164, 194–218.

Farmer, S., Alonsagay, M.E., Jarical, K.F., Primaleon, N.V., Libao, J.K., Pariña, E., Tucker, B.T., 2013. Long Chieng Track (LCT) Drilling Report Drill Programs 4B and 5A. PBM Internal Report. Phu Bia Mining office, Vientiane, pp. 111.

Gain, S., Gréau, Y., Murphy, R., Belousova, E., 2013. U-Pb Dating of Zircons from Samples: NS001 – NS002 – NS003. GEOMOC Report TC-117. Phu Bia Mining Limited, pp. 20.

Goldfarb, R.J., Collin, G.S., Goryachev, N.A., Orlandini, O.F., 2014. Phanerozoic continental growth and gold metallogeny of Asia. Gondwana Res. 25, 48–102.

Hedenquist, J.W., Arribas, A., Gonzalez-Urien, E., 2000. Exploration for epithermal gold deposits. In: Hagemann, S.G., Brown, P.E. (Eds.), Gold in 2000. Rev. Econ. Geol. 13, pp. 245–277.

Hoa, T.T., Anh, T., Phuong, N.T., Dung, P.T., Anh, T.V., Izokh, A.E., Borisenko, A.S., Lan, C.Y., Chung, S.L., Lo, C.H., 2008. Permo-Triassic intermediate–felsic magmatism of the Truong Son belt, eastern margin of Indochina. C. R. 340, 112–126.

Holcombe, R., 2012. In: Nam San and LCT Projects, Laos. Review of Current Structural Models. External report for Phu Bia Mining, pp. 17.

Hotson, M.D., 2009. The geochronology and tectonic framework of Cu-Au prospects in the Phonsavan district, northern Laos. Unpublished B.Sc (Honors) thesis. CODES, University of Tasmania, pp. 115.

Intasopa, S.B., Dunn, T., Lambert, R., 1995. Geochemistry of Cenozoic basaltic and silicic magmas in the central portion of the Loei-Phetchabun volcanic belt, Lop Buri, Thailand. Can. J. Earth Sci. 32, 393–409.

Irvine, T.N., Bargar, W.R.A., 1971. A guide to the chemical classification of the common volcanic Rocks. Can. J. Earth Sci. 8, 523–548.

Johnston, T., 2002. In: Geological Model LCT Gold Deposit, Lao PDR. Consultant report for Pan Mekong Exploration Pty Ltd, pp. 27.

Kamvong, T., 2013. Geology and Genesis of porphyry-skarn Cu-Au deposits of the Northern Loei and Troung Son Fold Belt. Unpublished Ph.D thesis. CODES, University of Tasmania, pp. 169.

Kosler, J., Sylvester, P.J., 2003. Present trends and the future of zircon in geochronology; laser ablation ICPMS. Rev. Mineral. Geochem. 53, 243–275.

Leaman, P.W., Tucker, B.T., Logan, K.J.F., 2015. The discovery of the Nam San copper-gold deposit, Phu Kham, Laos. In: PACRIM 2015 Congress, Hong Kong, China, 18th-21st March, 6 p.

Lepvrier, C., Maluski, H., Tich, V.V., Leyreloup, A., Thi, T.T., Phan, T.T., Nguyen, V.V., 2004. The Early Triassic Indosinian orogeny in Vietnam (Truong Son belt and Kontum massif); implications for the geodynamic evolution of Indochina. Tectonophysics 393, 87–118.

Libao, J.B., 2015. In: Base Metal-high Grade Au Zonation Analysis of the Long Chieng Track Prospect. Phu Bia Mining Internal Company Report, pp. 6.

Lin, T., Chung, S., Lo, C., Lan, C., Wang, P., Lee, T., Tran, T., Hoang, H., Tran, T., 2007. Implications for the Indosinian Orogeny and closure of eastern Paleo-Tethys: a perspective from the Song Ma suture. In: AGU, Fall Meeting, 2007, abstract V41D-0822.

Loucks, R., 2014. Distinctive composition of copper-ore-forming arcmagmas. Aust. J. Earth Sci. 61, 5–16.

Manaka, T., 2008. Geological setting and mineralisation characteristics of the Long Chiang Track and Ban Houayxai deposits, Lao PDR. Unpublished M.Sc. thesis. CODES, University of Tasmania, pp. 159.

Manaka, T., Zaw, Khin, Meffre, S., Vasconcelos, P.M., Golding, S.D., 2014. The Ban Houayxai epithermal Au–Ag deposit in the Northern Lao PDR: Mineralization related to the Early Permian arc magmatism of the Truong Son Fold Belt. Gondwana Res. 26, 185–197.

Mason, D.R., 1997. In: Petrographic Study of Eleven Drill Core Rock Samples from Long Chieng Track Deposit, Lao PDR. Mason Geoscience Pty. Ltd Consultants report for Phu Bia Mining Ltd, pp. 30.

Meffre, S., Khin Zaw, team, 2011. Tectonic models and ore genesis. In: Report for the implementation meeting of Ore Deposits of SE Asia Project, 17th October, 2011, Hobart, Tasmania.

Meffre, S., Scott, R.J., Glen, R.A., Squire, R.J., 2007. Re-evaluation of contact relationships between Ordovician volcanic belts and the quartz-rich turbidites of the Lachlan Orogen. Aust. J. Earth Sci. 54, 363–383.

Merriner, P., 2013. The discovery and geology of the Kham Thong Lai copper-gold deposit, Lao PDR. In: AIG Geoscientists Symposia, May 27th-29th, 2013 Bali, Indonesia, Extended Abstract, pp. 57–58.

Nakano, N., Osanai, Y., Owada, M., Nam, Tran Ngoc, Toyoshima, T., Binh, Pham, Tsunogae, T., Kagami, H., 2007. Geologic and metamorphic evolution of the basement complexes in the Kontum massif, central Vietnam. Gondwana Res. 12, 438–453.

Norman, M., Robinson, P., Clark, D., 2003. Major- and trace-element analysis of sulphide ores by laserablation ICP-MS, solution ICP-MS, and XRF; new data on international reference materials. Can. Mineral. 41, 293–305.

Norrish, K., Chappell, B.W., 1977. In: X-ray fluorescence spectrometry. Acad. Press, London, pp. 201–272.

PanAust, 2014. Mineral Resource and Ore Reserve Statements. Australian Stock Exchange Release.

Pearce, J.A., Harris, N.B.W., Tindle, A.G., 1984. Trace element discrimination diagrams for the tectonic interpretation of granitic rocks. J. Petrol. 25, 956–983.

Puthep Company limited, 2009. In: Puthep Copper Project Feasibility Study: Geology of the PUT 1 Copper Deposit. Puthep. Internal company report, pp. 69.

Salam, A., 2013. A geological, geochemical and metallogenic study of the Chatree epithermal deposit, Petchabun Province, Central Thailand. Unpublished Ph.D thesis. CODES, University of Tasmania, pp. 268.

Shi, M.-F., Lin, F.-C., Fan, W.-Y., Deng, Q., Cong, F., Tran, M.-D., Zhu, H.-P., Wang, H., 2015. Zircon U-Pb ages and geochemistry of granitoids in the Troung Son terrane, Vietnam: tectonic and metallogenic implications. J. Asian Earth Sci. 101, 101–120.

Sun, S.S., McDonough, W.F., 1989. Chemical and isotopic systematics of oceanic basalts: implications for mantle composition and processes. In: Saunders, A.D., Norry, M.J. (Eds.), Magmatism in the Ocean Basins. Geological Society Special Publication. 42, pp. 225–232.

Tate, N.M., 2003. In: Mapping Notes for the LCT Gold Deposit, Lao PDR. Consultant report for Pan Mekong Exploration Pty Ltd, pp. 19.

Tate, N, M., 2005. Discovery, geology and mineralization of the Phu Kham copper-gold deposit Lao Peoples Democratic Republic. In: Mao, J.W., Bierlein, F.P. (Eds), Mineral Deposit Research: Meeting the Global Challenge. Proceedings of the Eighth Biennial SGA Meeting Beijing, China, 18–21 August 2005, 2, pp. 1077–1080.

Wilson, M., 1989. Igneous Petrogenesis: A Global Tectonic Approach. Unwin Hyman, London.

Winchester, J.A., Floyd, P.A., 1977. Geochemical discrimination of different magma series and their differentiation products using immobile elements. Chem. Geol. 20, 325–343.

Wroe, J.A., 1997. In: Summary Technical Report for the Phonsavan Contract Area (January 1st 1994–31st December 1997). Phu Bia Mining Internal report, pp. 70.

Yu, Z., Robinson, P., Townsend, A.T., Munker, C., Crawford, A.J., 2000. Detection of geological materials for trace element determination of using ICP-MS. Geostand. Newslett. 25, 199–217.

Zaw, Khin, Meffre, S., Lai, C.-K., Burrett, C., Santosh, M., Graham, I., Manaka, T., Salam, A., Kamvong, T., Cromie, P., 2014. Tectonics and metallogeny of mainland Southeast Asia – a review and contribution. Gondwana Res. 26, 5–30.